Curtin

Centre for Marine Science and Technology

Internal Report

Hydrodynamic tests on a flat plate in forced oscillation

By:
Kim Klaka

HYDRODYNAMIC TESTS ON A PLATE IN FORCED OSCILLATION

CONTENTS

0   NOMENCLATURE

A	area (m^2)
AR	aspect ratio
b	semi-chord (m)
c	chord (m)
cp	centre of pressure
C_d	quadratic drag coefficient
C_m	inertia coefficient
C_y	sway force coefficient
C_z	heave force coefficient
C_φ	total roll moment coefficient
D	representative length (m)
f	frequency (Hz); force per unit length (Nm^{-1})
Fn	Froude number
g	acceleration due to gravity (ms^{-2})
h	distance from plate tip to bottom of channel (m)
KC	Keulegan-Carpenter number
k_i	equation of motion coefficient
M	roll moment (torque) (Nm)
p	length of free edge (i.e. immersed perimeter) (m)
Rn	Reynolds number
s	span (m)
t	thickness (m); time (s)
T	period (s)
u	reference velocity (ms^{-1})
UKC	dimensionless underplate (keel) clearance
w	dimensionless frequency
x	displacement amplitude at mid-span (m)
ω	radial frequency ($rad.s^{-1}$)
ν	kinematic viscosity (m^2s^{-1})
φ	roll angle (rad)
φ_a	roll angle amplitude (rad)
ρ	density (Kgm^{-3})

1   AIMS

The aims of the experiment were to

- Measure the hydrodynamic forces acting on flat plates oscillating in calm water.

- Determine the effect of plate profile shape and aspect ratio on hydrodynamic forces.

- Investigate the influence of underplate clearance.

- Identify the effect of oscillation frequency and amplitude on hydrodynamic forces.

2   BACKGROUND

2.1   A note on terminology

The research described was conducted by the author whilst enrolled in a doctoral program in the Department of Applied Physics at Curtin University. The topic lies in the field of naval architecture, generally considered a branch of engineering for the most part. The terminology adopted is that most commonly used in naval architecture and, where practicable, symbols and sign conventions follow the recommendations of the International Towing Tank Conference (Johnson, 1999). In an endeavour to make this work accessible to a readership in the fields of both engineering and science, some of the terms used are described below in greater detail than might be found in work pertaining to a single discipline.

- Motions

There are three degrees of freedom of motion pertinent to the current work, shown in Figure 2-2. Sway is lateral displacement, heave is vertical displacement and roll is angular displacement about the longitudinal axis. The origin is on the vessel centreline at the still water level and a right handed axes convention is used. This differs from some naval architecture work in which the origin is body-fixed, at the centre of gravity of the vessel.

- Torque and moment

The torque generated by a force may be called a moment, and is done so in this work. For example, the torque associated with the roll motion of a vessel is called the roll moment. This is distinct from the mass moment, which is defined in the next section.

- Mass moment and moment of inertia

The second moment of mass of an object is called the mass moment of inertia. This is distinct from the moment generated by a force creating torque (see above).

- Plate geometry

For the current work, the span may be considered the same as the depth and the chord equivalent to the width (Figure 2-1). The geometric aspect ratio of an object is defined as the square of the span divided by the area normal to the flow. For rectangular objects this reduces to span/chord. The effective aspect ratio takes into account the mirror image of the object about an attached boundary. For a solid boundary at one tip of the object, the effective aspect ratio will be twice the geometric aspect ratio. If there is no boundary at either tip, the effective aspect ratio is the same as the geometric aspect ratio.
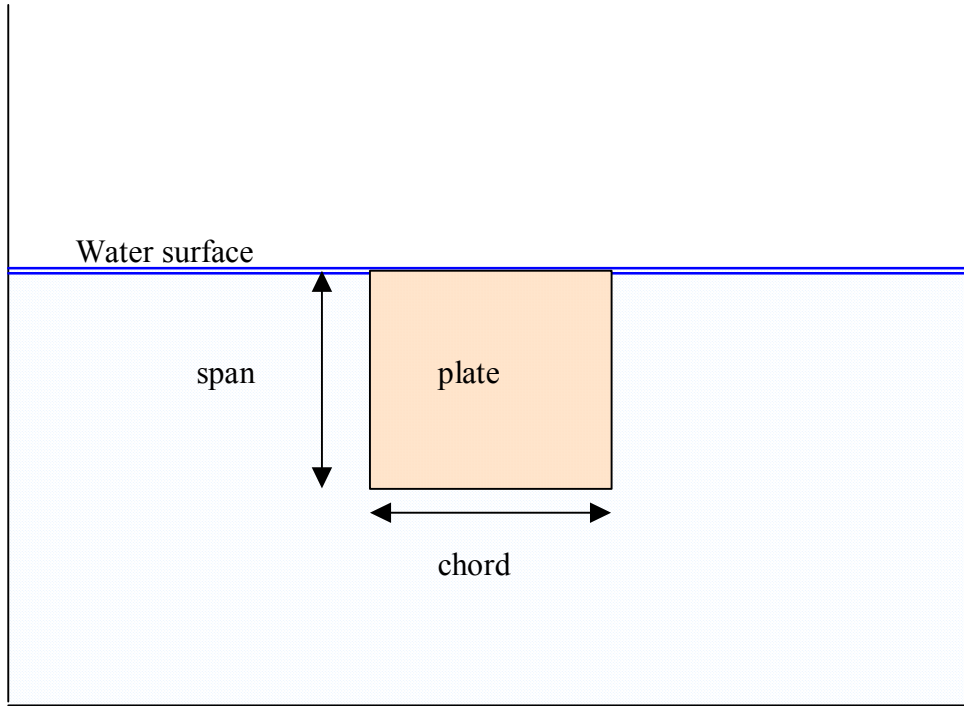
Figure 2-1 Plate geometry definitions
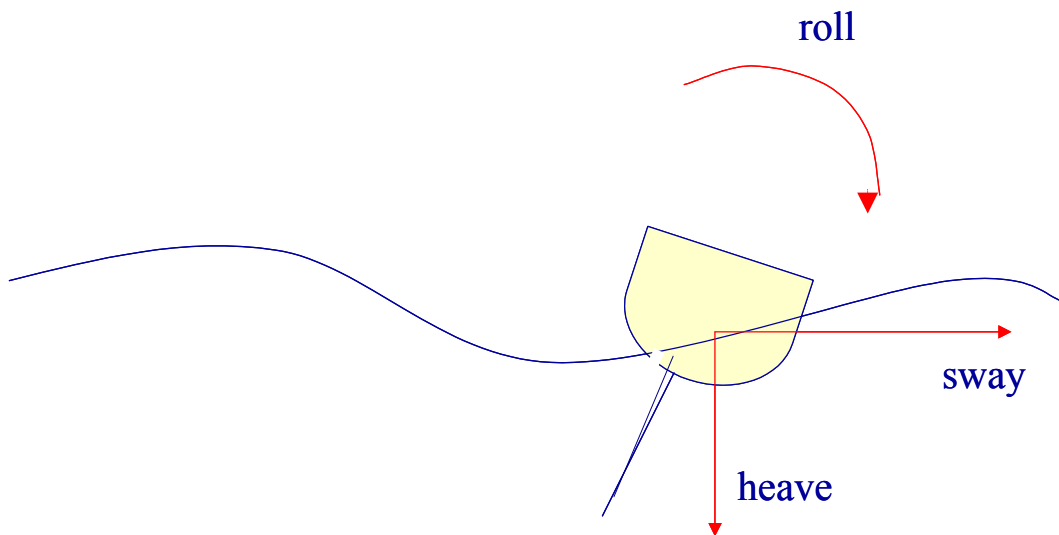
Figure 2-2 Motion definitions for a rolling yacht.

2.2   Previous work

A research program is being conducted to predict the roll motion of a sailing yacht at zero ship speed in a low amplitude ocean wave field, in both deep and shallow water. Shallow water effects were considered important because yachts tend to anchor relatively close to shore when seeking shelter, and are thus frequently rolling in water depths less than twice the vessel draft. Roll motion prediction for large ships is understood to be the consequence of both viscous and inviscid flow phenomena. The contribution of the hull shape to roll damping as determined from inviscid flow analysis is quite large, as a consequence of the hull cross sectional shape and the relatively small size of appendages. On the other hand a sailing yacht has a canoe body of cross-sectional shape more closely approximating that of a circular section and, more significantly, the size of the appendages is proportionally much larger than for a ship. Consequently, the roll motion is not well predicted by inviscid theory. Computer predictions by the author, backed up by full scale and model experiments, confirmed that the roll damping for a sailing yacht was dominated by the keel, rudder and sail rather than the canoe body (Klaka, 2000, Klaka, 2001a, Klaka, 2001b). It was also shown that these appendages could be considered as 3-D flat plates oscillating in rotational motion.

One of the earliest comprehensive experiments on oscillating flat plates (Keulegan and Carpenter, 1958) was conducted in a small basin in which a standing wave was generated. The experiments were conducted both on circular cylinders and flat plates. The plate was stationary and the flow motion was approximately normal to the plate (the term linear is often used to describe this, but is easily confused with mathematical linearity with respect to motion amplitude). The plates and cylinders were submerged at least 3 diameters below the free surface.

Another technique widely used is to place a plate or cylinder in a U-tube and then vary the oscillation amplitude at constant frequency so as to generate a linear oscillation of the flow (Bearman et al., 1985), (Sarpkaya and O'Keefe, 1995). There is no free surface effect in the working part of the U-tube.

(Ridjanovic, 1962) conducted tests on a series of flat plates of varying aspect ratio. They were suspended a long way below a pivot, and connected to a pendulum. The pendulum was displaced and the hydrodynamic force determined from the angle decay rate. The plates therefore underwent a combination of linear and rotational motion, but the plates were three-dimensional and therefore of potential relevance to the current investigation.

During the 1990s Yeung developed a computational method for estimating the forces on a rotating oscillating plate pivoting at the free surface, albeit in 2-D dimensional flow, and conducted validation experiments (Yeung et al., 1997), (Yeung et al., 1998).

A review of the literature revealed a dearth of experimental data on forces and moments generated by 3-D flat plates in rotational oscillation at various water depths. In order to proceed further, a forced rotational oscillation rig was designed and built to address this deficiency.

3   METHODOLOGY

3.1   **Design requirements**

The experiment was required to show the effects of underkeel clearance and plate geometry on the hydrodynamic forces and moments generated by the plate motion.

The plate motion had to replicate that of a yacht keel in pure roll motion. Given that a vessel pivots approximately about its centre of gravity at small roll angles (Lewis, 1989), and that the centre of gravity for many yachts is close to the waterline (Larsson and Eliasson, 1994), (Kinney, 1973), the hinges for the plates in the experiment were located at the still water level. The hinge bearing material had to be of low friction and not influenced by water immersion.

The measurements had to allow for the possibility of channel end-reflections from any generated waves, which placed a constraint on the duration of data sampling at a given oscillation frequency for a given length of water basin. In practical terms this meant that the length of the basin had to be at least 20 times greater than the representative plate length.

The driving mechanism for the plate motion had to be of variable frequency with low noise and exhibit a very fast acceleration. The latter requirement was crucial if an adequate sampling duration was to be achieved, because a long transient would tend to generate a low frequency component of free surface elevation which would have a very short reflection time. For the frequency range under consideration, the waves generated were all intermediate depth waves i.e. neither the deep nor the shallow water approximations applied. A DC electric motor was chosen to activate the drive mechanism.

The motion of the plate was chosen to be a close approximation to sinusoidal. Whilst ocean waves generate a pseudo-random roll motion, the theory of superposition has been successfully applied to small angle motions analysis and seakeeping model experiments (Lloyd, 1989), (Bertram, 2000). The plate motion was not a true sinusoid because the choice of a crank arm attachment – a concession to mechanical simplicity – introduced geometric variations which resulted in a small deviation from pure sinusoidal motion.

The inertia of the plate had to be kept to a minimum in order to prevent the loads induced by acceleration of the plate (as distinct from the surrounding water) from dominating the signals. Similar constraints on buoyancy force required the plates to be thin, though sufficiently stiff to retain their planar form under load.

The results were required to be input to the single degree of freedom time domain computer program written by the author (Klaka, 2001b). This was written to output time domain roll motion of a yacht driven by sinusoidal free surface gravity waves. The appendages in the model were treated as fully submerged flat plates and calculation of the forces acting was based on a stripwise Morison formulation (Chakrabarti, 1987). It was envisaged that the output from the proposed experiment would be used to modify the Morison coefficients. The revised model could then be used for comparison with wave basin tests (Klaka, 2001a) and full scale trials (Klaka, 2000).

The results also had to be in a format suitable for comparison with results by other researchers. The format chosen was time series of the heave and sway forces, roll moment and plate angle. Statistical summaries of the time series were also determined.

3.2   Scaling

The plate forces are a function of both Keulegan-Carpenter number (KC) and Reynolds number (Rn):

$$KC = \frac{uT}{D}$$ (1)

$$Rn = \frac{uD}{\nu}$$ (2)

where

u = representative velocity

T = period of oscillation

ν = kinematic viscosity

D = representative length

where free surface gravity waves are present, the Froude number (Fn) is also influential:

$$Fn = \frac{u}{\sqrt{gD}}$$ (3)

The choice of representative velocity u and length D depends on the nature of the problem under investigation. (Yeung and Cermelli, 1998) conducted research on oscillating two-dimensional flat plates in waves. They used the distance travelled by the plate tip as the representative length, and the maximum velocity of the plate tip for the representative velocity, yielding:

$$Rn_{Yeung} = \frac{2\varphi_a^2 \omega s^2}{\nu}$$ (4)

where

φ_a = roll angle amplitude

$$\omega = \frac{2\pi}{T}$$

s = plate span (see *Figure 4-1*)

For the present work, the span was considered a representative length, and the velocity amplitude at the tip was used as the representative velocity. This yielded a Reynolds number of :

$$Rn_{Klaka} = \frac{\varphi_a \omega\ s^2}{\nu} \tag{5}$$

Clearly, care must be taken when comparing results from different sources.

A slightly different problem arises when considering appropriate quantities for Keulegan-Carpenter number. (Yeung and Cermelli, 1998) used plate thickness as the representative length dimension and maximum tip velocity as the representative velocity. This yielded:

$$KC_{Yeung} = \frac{2\pi\varphi_a s}{t} \tag{6}$$

where

t = plate thickness

An appropriate length scale for the current work was considered to be the plate span and the reference velocity was the maximum velocity at the plate tip. For a flat plate pivoting along its top edge and oscillating sinusoidally, the reference velocity is then:

$$u = \frac{2\pi s\varphi}{T} \tag{7}$$

so

$$KC = \frac{2\pi s\varphi}{sT}T \tag{8}$$

$$= 2\pi\varphi$$

This does not relate the KC to the frequency of oscillation; instead, a dimensionless frequency must be used. A Froude based frequency scaling was used, using the plate span as the reference length:

$$w = \omega\sqrt{\frac{s}{g}} \tag{9}$$

where

w = dimensionless frequency

ω = radial frequency of oscillation

Under Froude scaling the inertial effects will be correctly scaled. The Reynolds number will change but the effects are usually quite small if there is a significant amount of separated flow and the separation points do not change position with Reynolds number (Hoerner 1965), (Hoerner and Borst 1975). In such circumstances the non-dimensionalised forces and moments may be compared directly for experiments conducted at the same Froude number. Nevertheless care should be taken when comparing results from experiments conducted at significantly different Reynolds number. Further, caution is urged to check that the non-dimensionalising parameters used are the same. Forces and moments are non-dimensionalised as follows:

$$C_z = \frac{heave\ force}{\frac{1}{2}\rho A u^2} \qquad (10)$$

$$C_y = \frac{sway\ force}{\frac{1}{2}\rho A u^2} \qquad (11)$$

$$C_\varphi = \frac{roll\ moment}{\frac{1}{2}\rho A u^2 s} \qquad (12)$$

where

A = plate profile area

ρ = water density

u = maximum velocity at plate tip

s = plate span

The two dimensionless numbers used for scaling force and moment coefficients were therefore roll amplitude φ and dimensionless frequency w.

3.3   Parameter space

The parameter space investigated was determined largely by the range of angle amplitudes, dimensionless frequencies and keel shapes of the wave basin tests (Klaka, 2001a) and full scale trials (Klaka, 2000), and as far as practicable the 2-D experiments of (Yeung et al., 1997), see Table 3-1.

test	parameter	Range from	to
benchmark (Yeung 1997)	φ (deg)	5	15
full scale trials (Klaka 2000)	φ	0	15
model tests (Klaka 2001)	φ	0	15
Current work	**φ**	**0**	**20**
benchmark (Yeung 1997)	w	0.28	0.63
full scale trials (Klaka 2000)	w	0.34	0.91
model tests (Klaka 2001)	w	0.44	1.32
Current work	**w**	**0.15**	**2.0**
benchmark (Yeung 1997)	Rn_{Yeung}	3.2E3	2.9E4
benchmark (Yeung 1997)	Rn_{Klaka}	1.4E4	9.6E4
full scale trials (Klaka 2000)	Rn_{Klaka}	8.0E4	6.8E5
model tests (Klaka 2001)	Rn_{Klaka}	3.7E3	1.8E4
Current work	**Rn_{Klaka}**	**2.9E2**	**1.8E5**

Table 3-1 Parameter space constraints

Four plates were tested (see Table 4-1 for details):

- *Plate 1:* a full width rectangular flat plate, of infinite effective aspect ratio (c/f (Yeung et al., 1997))

- *Plate 2:* a square plate (c/f (Klaka, 2001a)).

- *Plate 3:* same area as plate 2, but double span

- *Plate 4:* same chord as plate 2 but double span

3.4   Inertia and drag coefficients

The Morison equation for a stationary object in oscillating flow is (Keulegan and Carpenter, 1958)

$$f = C_m \rho \frac{\pi}{4} D^2 \frac{\partial u}{\partial t} + C_d \frac{\rho}{2} D |u| u \qquad (13)$$

where

f = force per unit length across the flow

C_m = inertia coefficient

C_d = drag coefficient

D = representative length

u = instantaneous local fluid particle velocity

The equation of motion for a plate undergoing forced angular oscillation may be written as:

$$M = k_1 \ddot{\varphi} + k_2 \dot{\varphi} |\dot{\varphi}| + k_3 \dot{\varphi} + k_4 \varphi \qquad (14)$$

where

M = moment generated by plate

φ = roll angle

$\dot{\varphi}$ = roll angular velocity

$\ddot{\varphi}$ = roll angular acceleration

k_i = moment coefficients

The coefficients k_3 and k_4 are often assumed to be zero, revealing a straightforward relationship between the remaining coefficients k_1 and k_2 of the motion equation and the inertia and drag coefficients respectively of the Morison equation. There are several ways of

computing the equation coefficients, the method chosen being the least squares technique (Chakrabarti, 1987) p192.

4   EQUIPMENT

4.1   **Water channel**

The facility used was an Armfield Engineering S5-10 circulating open water channel, with a 10m long working length of cross section 300mm square. The sides were transparent. The ends of the channel were blocked off for these experiments and the channel filled with water to the desired level.

4.2   **Plates**

The plates were made of 6mm Perspex with square edges. The plate dimensions are shown in *Table 4-1*. The 2-D plate (plate 1) had gaps of 3mm at each end between the plate and the channel wall.

Plate 1

Plate 2   Plate 3   Plate 4
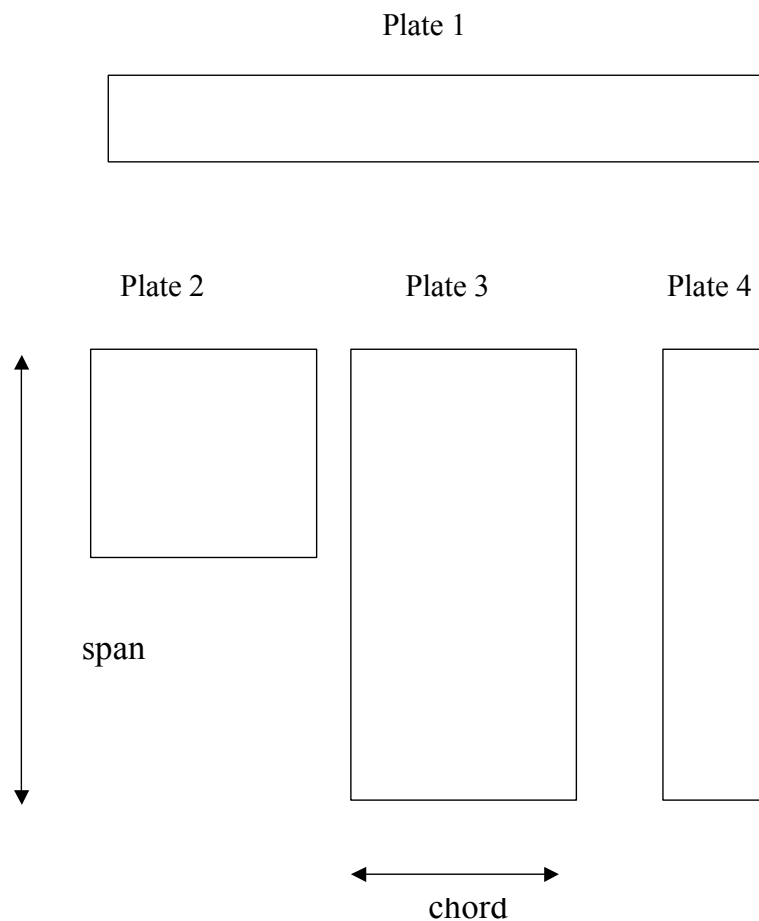
span

chord

Figure 4-1. Plate profiles

	Plate 1(2-D)	Plate 2	Plate 3	Plate 4
mass (Kg)	0.105	0.075	0.151	0.069
Immersed span (m)	0.042	0.091	0.20	0.20
Chord (m)	0.294	0.10	0.10	0.0455
Area (m^2)	0.012348	0.0091	0.02	0.0091
Geometric aspect ratio	0.143	0.91	2	4.4

Table 4-1 Plate geometry

4.3   Rig

The attachment rig for holding the plates comprised two horizontal aluminium base-plates connected by vertical rods (Figure 4-2 and Figure 4-3) . The upper base was clamped to the sides of the channel. The hinge supports, crank and crank arm were attached to the lower base. The lower base could be moved up and down relative to the upper base to enable tests to be conducted at different water depths whilst keeping the plate hinge at the static water level. The hinge supports could be adjusted transversely to accommodate plates of varying width (chord). The plate was connected to a crank arm and electric motor, the speed of which was controlled in analogue form from the power supply. The motor was connected via stacks of planetary gears which could be changed in order to alter the gearing ratio. The crank arm could be altered to yield angle amplitudes from 7.5° to 20° in 2.5° steps. The crank arm length was adjustable to account for the small changes in geometry accompanying a crank offset change. A friction brake was fitted to the gearbox drive shaft to reduce backlash in the drive train.
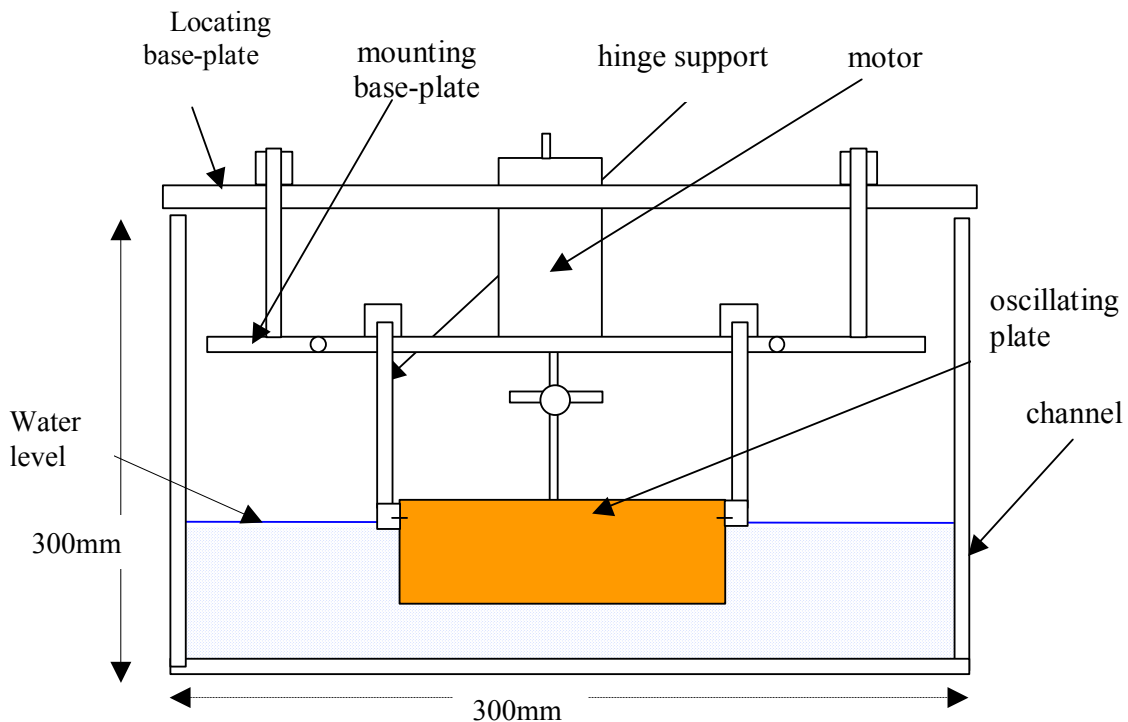
Figure 4-2 End view of rig
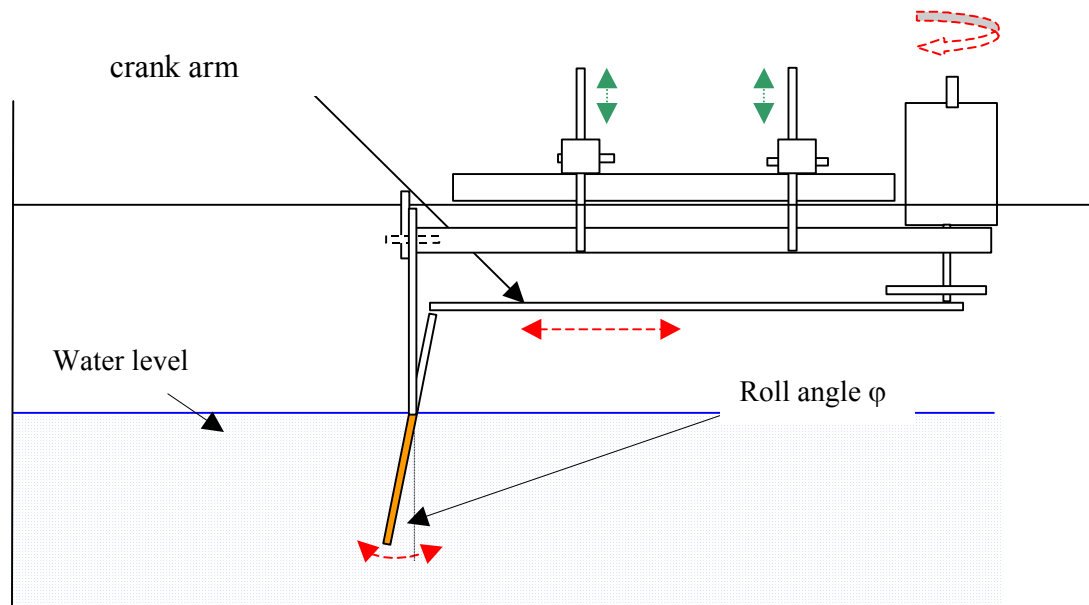
Figure 4-3 Side view of rig

4.4   Instrumentation

The instrumentation for these experiments comprised 12 strain gauges (see 4.5) and a rotary potentiometer. The rotary potentiometer measured the position of the crank attachment by way of a length of twine run over a pulley then three wraps round the potentiometer wheel to a small lead mass. The lead mass was made as small as possible (0.0145Kg) to minimise inertia whilst maintaining the twine in tension under the dynamic conditions likely to be experienced. Measurement of the plate motion could have been achieved by measuring motor speed and working through the gearing and crank geometry. However, it was considered important to ensure accurate and reliable synchronisation of the motion with the loads so the motion of the plate was measured directly with a rotational potentiometer. Use of this method came at the expense of increased inertia from the potentiometer connection.

The Daqbook system (IOtech, 2000) was used for data acquisition and signal conditioning, connected to a PC.

4.5   Strain gauges

The gauges were super-glued to the aluminium substrate then coated in polyurethane. The hinge supports were strain gauged as shown in Figure 4-4. The upper pair were connected as a half-bridge to provide a difference reading for maximum sensitivity to sway-induced bending moment. The signals from the lower pair were recorded individually in order to measure heave force. The transverse gauge provided a check on sway force measurement (through Poisson strain) and any torsional load. Whilst this configuration did not permit decomposition of the readings into all possible load conditions, it did allow for checks to be made for contamination of signals from unexpected load conditions. Cross-axis sensitivity of the gauges was measured during calibration and showed that measured strains were parallel to the plane of the tank. This simplified the analysis, as the heave and sway components from each gauge could be treated as scalar quantities. The crank attachment was gauged with

a half bridge pair, based on the assumption that the only dynamic load was in line with the crank arm because it was fitted with a ball joint attachment.
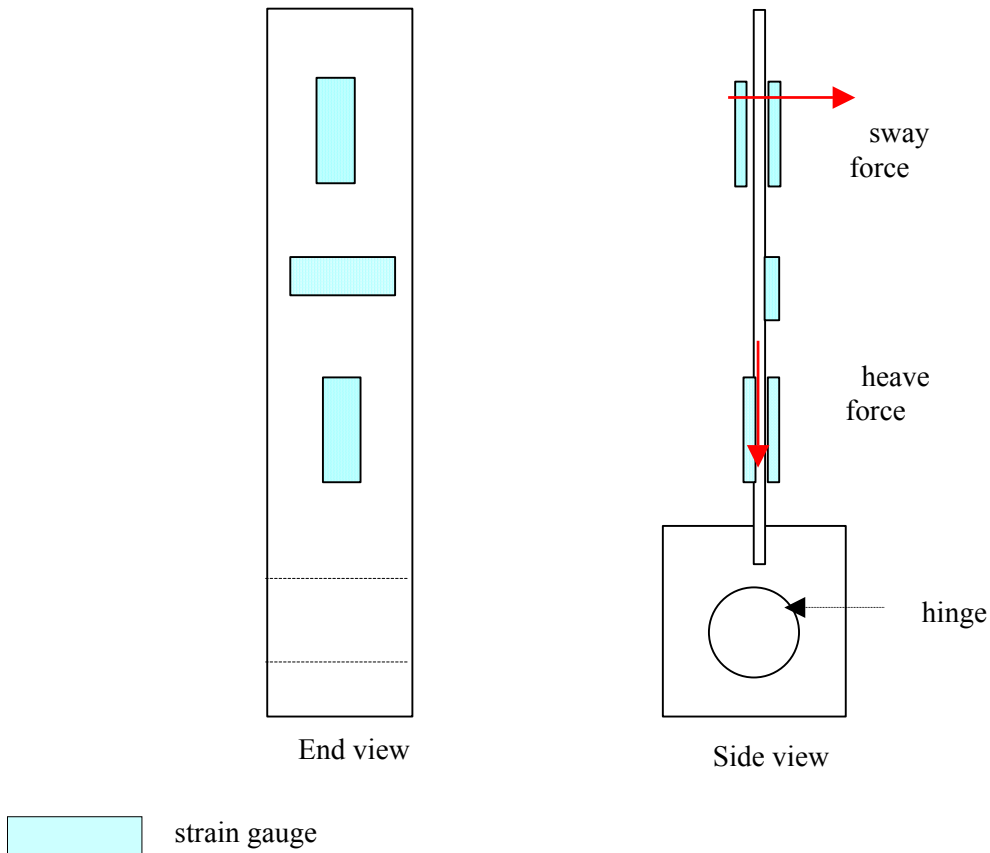
Figure 4-4 Hinge support gauge configuration

5   PROCEDURE

5.1   Calibration

The strain gauges were calibrated statically by applying known loads to each hinge support and the crank arm connection, for a number of directions over a range of amplitudes. The load took the form of a mass attached to twine which was run over a pulley to the gauge platform of interest. The mass motion was allowed to stabilise for a few seconds then the mean value of the gauges over typically 5 seconds was recorded. These mean values were plotted and a linear regression of load against voltage performed in order to determine the calibration factor. The offset was not required for calibration as only dynamic force measurements were required. The calibration process was conducted at two different gain settings for the strain gauges. The maximum load applied was limited by the deflection of the gauge support being large enough to jeopardise the integrity of the bond between gauge and substrate. The air temperature during calibration was 21°.

The potentiometer was calibrated by relating its full scale output to the circumference of the potentiometer wheel. A check was made against plate angle as measured with a protractor.

5.2   Test runs

The strain gauge circuits were allowed to warm up for typically one hour in order to reduce gauge drift due to temperature variation. For tests in air, prior to each run the bearings were sprayed with water to simulate the friction characteristics of an in-water test. The temperature of the water was 20°.

Data acquisition then started, for 20 seconds duration. The duration of the tests in water was limited by the time taken for any generated waves to be reflected from the tank ends back to the plate. The interval between in-water runs was determined by the time taken for any generated waves to die down – approximately 5 minutes.

During each run the digital display of signals was inspected and if a channel reached saturation that run would be discarded, the gains reduced if appropriate, and the run repeated. Runs where readings extended beyond the limits of calibration were also discarded.

Photos and video footage were taken at various times during the tests.

5.3   Data Processing

The required output of the data processing was time series of hydrodynamic forces and moments. The total forces and moments measured comprised contributions from hydrodynamic effects, equipment inertia and bearing friction. These latter two had to be removed from the total signal in order to isolate the hydrodynamic effects. This was achieved by subtracting the in-air run results from the equivalent in-water results, on the assumption that the in-air runs comprised only inertial and friction effects of the same magnitude as for the in-water run. This process was particularly important for the low frequency runs, where the in-air component of the total signal was of similar magnitude to the hydrodynamic component.

All signals acquired were analogue DC, digitised at 100Hz. The Daqbook system was used, with analogue low pass 3rd order Butterworth anti-aliasing filters set at 20 Hz. The mean values of every signal for each run were then zero-meaned and a digital 10Hz low pass Butterworth filter applied. The driving frequency was then determined from the zero upcrossing points and the time series truncated to an integer number of cycles. This truncated signal was zero-meaned again then Fourier transformed. Spectral components below 0.2Hz were discarded and the spectrum inverted. The instrument calibration factors were then applied, and the total sway, heave and roll moment determined from the individual gauges as follows:

Sway was calculated as the sum of the horizontal forces from :

- Left and right lower hinge support gauge pair and

- crank support gauge pair

The heave was then calculated from the average of signal from the upper gauges on the hinge supports in a series of steps:

- The sway component of the signal at these gauges was determined from the sway force calculated in the preceding step,

- then subtracted from the gauge signal

- and the residual converted to heave.

- The heave force from the left and right gauges were added to get the total heave force.

The roll moment was determined by taking moments about the hinge support.

From this point on, the data processing for the in-air and in-water tests differed. The in-air signal had to be subtracted from the in-water signal, but it was not possible to conduct the two sets of tests at exactly the same frequencies because the motor speed setting could not be replicated exactly. Therefore the in-air time series were modelled as the first 10 harmonics of the associated Fourier series, then normalised.

For the in-water tests, the equivalent in-air signal was subtracted by reading in the Fourier model of the in-air tests for all oscillation frequencies, interpolating the Fourier coefficients for the correct in-water frequency, reconstructing the interpolated model time series and subtracting it in the time domain from the in-water signal. The analytically derived buoyancy correction was then applied to the roll moment signal. It did not affect sway force and was only a DC offset for the heave force. The frequency and standard deviation of the resulting signals were output to a summary file in both dimensional and dimensionless form, and the force, moment and motion time series stored in a separate file.

The drag and inertia coefficients were obtained from the time series using a least squares technique solving for minimisation in deviations of squares of values in matrix *B* for fixed values of matrix *X* in the equation:

$$AX = B$$ (15)

6   ERRORS

6.1   Strain gauge signals

Only dynamic measurements of strain were required, so problems with slowly varying offsets were not important, except for the calibration process. The physical size of the rig components were small relative to the size of the gauges, so there were errors due to strain gradients, gauge thickness etc. However, these were largely accounted for in the calibration process. Temperature effects were accounted for in two ways. Firstly, by choosing gauges with a thermal expansion coefficient similar to that of the attachment plate. Secondly, by taking measurements over short duration, which were thus unlikely to experience significant change in temperature.

The signal generated by a gauge may be the resultant of strains in several different directions. The gauge configuration reduced this contamination and enabled checks to be made on its extent. For example, the transverse gauges on the hinge support would respond to both sway force and torsion (and to a much lesser extent, heave force and any cross-channel signal), whereas the differenced upper gauge pair signal was dominated by strain induced by sway force. Therefore a check for excessive torsion could be made by comparison of the signals from the upper pair and the Poisson-strain from the transverse gauge. However, this was not a suitable method for measuring such loads as there was cross-contamination and large errors; rather it provided a useful data quality check on a pass-fail basis.

The heave force signal was generated by the axial load in the hinge supports and determined from the average reading from each of the lower pair of gauges on the hinge supports (see 5.3). The absolute strain values were very low, owing to the necessary stiffness of the supports. Consequently the errors in the heave-induced signal were very large – over 50% in many instances.

6.2   Strain gauge calibration

The coefficient of determination (r^2) for the calibration factors used to determine the sway force and roll moment were always greater than 0.999. Cross-coupling between gauges was measured and found to be insignificant, except for the quantifiable instances of Poisson strain. Temperature fluctuations may have affected the calibration factors, though the gauge specifications indicate this would be an error of second order magnitude over the temperature range of the experiments.

6.3   Blockage

An object placed in a channel will experience different forces compared with the same object placed in unrestricted flow. This effect is known as blockage, and is reasonably well understood in wind tunnels (Rae and Pope, 1984), (Pankhurst and Holder, 1965) and towing tanks (Scott, 1976), (Harvald, 1983). The blockage effects for this experiment are related to, but not the same as wind tunnel effects and towing tank effects.

Blockage effects may be divided as follows:

Wall boundary layer effects.

The progressive thickening of the boundary layer along the length of the channel wall causes a decrease in the static pressure downstream, hence a drag increase. This effect is important in wind tunnels but is considered negligible for water tests because the boundary layer thickness is proportionally much smaller.

Solid blocking

The presence of the plate in the channel reduces the area through which water may flow. For a closed channel e.g. a wind tunnel, the effect is much less than (approximately 25% of) the amount calculated by applying Bernoulli's equation, despite the average velocity change being accurately predicted. This is because the change in streamlines is greater as you move further away from the plate, but the forces related to that change decrease with distance from the plate. The mathematical approach to calculating solid blockage is by the method of images, using doublets. This method becomes quite complicated when a free surface is present, and is not considered suitable for this experiment. Given that the free surface provides a pressure relief, the wind tunnel solid blocking calculations provide an upper threshold estimate of this blockage component, rather than an accurate estimate.

Wake blocking

The mean velocity in the wake will be lower than the free stream velocity; however, the velocity outside the wake in a closed channel must be higher than the free stream in order to maintain continuity of volume flow rate. This higher velocity will, from Bernoulli's theorem, decrease the pressure in the wake region and create an additional drag force. This is computed for wind tunnels by using a line source (across the channel) to represent the wake-generating trailing edge. The simulated wake is contained within the channel by adding an infinite vertical row of source-sink combinations, producing a net horizontal velocity. As with solid blocking, this method is not practical when a free surface is present, rather it provides an order of magnitude upper value estimate of the wake blockage.

Streamline curvature

The curvature of streamlines that occurs around any lifting body is restricted by the top and bottom of the channel. This results in an increase in lift compared with the unconstrained flow condition. For this experiment, the free surface yet again relaxes this constraint. The lift generated is very small for the conditions under investigation , so this blockage component has not been calculated.

Wave resistance blockage

The wave pattern generated by the plate will be affected by the channel boundaries, particularly the channel bed. This form of blockage is addressed in ship towing tank resistance tests, but in a manner inapplicable to this experiment for the following reasons:

- The methods, all empirically based (e.g. (Scott, 1976), (Scott, 1966)), include all blockage effects in one – including wake and solid blockage.

- The formulae used are based on ship length, a length dimension not appropriate to a plate normal to the flow

This experiment lies outside the range of data used to develop the empirical blockage formulae with particular regard to object slenderness and channel aspect ratio. This latter is surprisingly important, as shown the first data subset of table 1 in (Scott, 1976).The constraints of operating in an enclosed channel will influence the flow; this effect is known as blockage. It has been extensively investigated for wind tunnel and towing tank experiments ((Rae and Pope, 1984), (Scott, 1976)). However, wind tunnel blockage corrections do not apply to tests with a pressure-relieving free surface, and towing tank blockage corrections are largely focussed on surface wave effects and small ratios of model cross sectional area to tank cross sectional area. Given the uncertainty in estimating blockage effects for the current experiment, the results have been left uncorrected. This should be borne in mind when comparing with experiments conducted in facilities with different model:tank area ratios.

6.4   Other errors

Water depth was measured using steel rules permanently mounted on the outside of the channel. The measurement was accurate to within 1mm, but the level occasionally fluctuated from the target value by up to 2mm owing to operational difficulties.

The mean water temperature of 26.3°C varied by +-0.9°C over the period of the tests.

The plates were subject to slight flexure, so they did not remain planar in the dynamic condition. There may have been up to 2% camber induced through flexure. The plate motion was not exactly sinusoidal owing to the crank arm geometry introducing small variations (less than 1%). This was not an experimental error as such, rather a deviation from the assumed mode of motion.

The use of a crank also resulted in an off-axis loading (changing direction throughout the cycle), which caused variations in readings between the left and right gauges. There was approximately 1mm of lateral freedom between the plate and the hinge support during operation; during operation the plate would tend to move across to one hinge support and stay there, causing further discrepancies between the left and right gauges. Most of the error caused by these asymmetric loads was accounted for in the left-right averaging.

The friction in the bearings for the tests in air was unlikely to be the same as for the test in water at the same frequency, because the bearing load was different.

6.5   Error estimation and propagation

The error estimate comprised the following components:

- in-water signal

- in-air correction signal

- buoyancy correction (roll moment only)

Errors for the in-air signals were estimated firstly from the variance of the signal standard deviation for repeated runs, secondly by calculating the variance of the mean of the signal peak values within a run. Errors for the in-water signal were estimated only from variance of the mean of the signal peak values within a run. The errors from these sources were propagated through to the forces and moments, and finally to the dimensionless coefficients. A summary of error magnitudes for roll moment is given in Table 6-1; sway errors were of similar size. The percentage errors are similar for inertial, drag and total roll moment coefficients. The heave force error estimation was not investigated in as much detail because heave force estimation was not the main aim of the experiments, the rig not being designed for accurate heave force estimation. Heave force errors were difficult to estimate accurately, but appear to be up to 50% for most conditions, probably higher for the low frequency tests.

	Low frequency (0.5Hz)		High frequency (2Hz)	
	Plate 1	Plate 2	Plate 1	Plate 2
Dimensionless frequency w	0.2	0.3	0.83	1.2
Standard deviation of total roll moment (Nm)	2.5E-4	2.3E-4	3.1E-4	2.3E-4
Standard deviation of total roll moment as % of signal standard deviation	24%	9%	3%	0.5%
Standard deviation of total roll moment coefficient	1.4	0.3	0.06	0.03
Standard deviation of total roll moment coefficient as % of coefficient	25%	9%	4%	2%

Table 6-1 Error estimates for 12.5° roll amplitude

The errors in instrument calibration were two orders of magnitude less than other error sources. It was clear from the error propagation that the relative values of the errors were greater at lower frequencies because the amplitude of the in-air and buoyancy corrections were then of the same order as the in-water signal. The largest source of error for most

conditions was from the buoyancy correction. The principal source of error in the buoyancy correction was due to the variation in the water level with respect to the hinge height. This was greatest for the plates with longest chord and shortest span.

The conversion for force and moments into their respective coefficients introduced further errors. The greatest of these was in the velocity term, estimated from the potentiometer signal and the span measurement.

7   RESULTS AND DISCUSSION

7.1   **General observations**

The results shown in this report have been selected as a representative sample of the whole data set, in the interests of brevity and clarity of presentation. Trends evident in the roll moment were reflected in the sway force. The heave force results were unreliable owing to the low axial strain levels in the hinge supports. However, the focus of the work was on roll moment.

A typical time series of total hydrodynamic roll moment is shown in Figure 7-1. It exhibits an approximately sinusoidal wave form of consistent frequency and reasonably consistent amplitude. The standard deviation of the signal was used as a measure of magnitude, rather than the amplitude. This was considered a more representative quantity for a time varying signal, using more of the data in its estimate and because the data sets had been zero-meaned and de-trended.
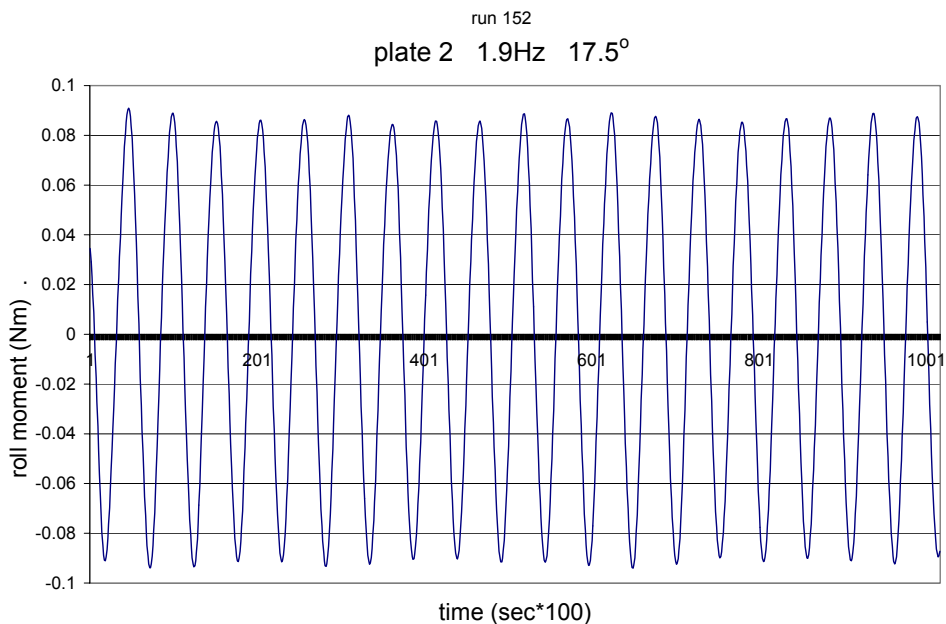
Figure 7-1 Typical total roll moment time series

7.2 Comparison with other work

(Ridjanovic, 1962) presented results for plates of varying aspect ratio as a plot of drag coefficient as a function of a modified Keulegan-Carpenter number (KC). His drag coefficient was in fact a total sway force coefficient, comprising both drag and inertial terms, and was thus directly comparable with the sway force coefficient from the tests described herein. His modified KC was the ratio of the displacement amplitude of oscillation at mid-span (x) to the half-width of the plate (b). His results were not directly comparable because the pivot point for oscillation was far above the plate, whereas the pivot point in the tests described here was at the top of the plate. In addition to the resulting difference in plate trajectory, the influence of aspect ratio was different. The conditions for the Ridjanovic tests were such that the results for a plate of aspect ratio r were almost the same as for a plate of aspect ratio 1/r. This was clearly not the case for the present tests. Further, the plates in Ridjanovic tests were suspended from a stalk and situated well below the free surface The present work, on the other hand, was conducted with the plates piercing the free surface. The free surface acts as a partially reflecting boundary – a solid surface would provide full reflection, increasing the effective aspect ratio of an abutting plate by a factor of 2 over the geometric aspect ratio. The pressure relieving influence, reduces the factor to somewhere between 1 and 2. Consequently, the comparison had greatest validity for a Ridjanovic plate of aspect ratio between 1 and 2. Figure 7-2 below shows good general agreement for these aspect ratios, and also illustrates that the current tests were generally at much lower KC number. Given the differences in experimental conditions, the comparison with Ridjanovic's work provides general support for the validity of the current experiment.
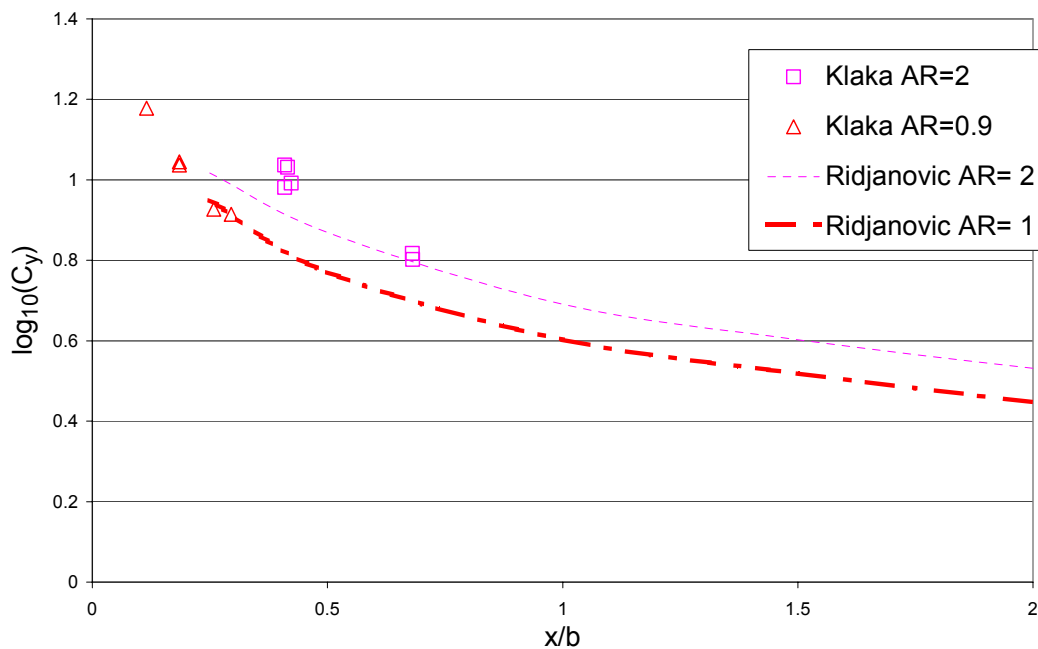
Figure 7-2 Comparison of results with Ridjanovic

The tests on the 2-D plate (plate 1) may be compared with the experimental work of (Yeung et al., 1997) on a plate of similar shape but approximately eight times larger. Aside from the effect of Reynolds number change, the scaling of the results depends on the relative contributions of the inertial and drag terms – the inertial term is proportional to angle amplitude whereas the drag term is proportional to angle amplitude squared. Using an

assumption of linearity, the results of Yeung et al at 10° amplitude were scaled to the current results at the nearest angle amplitudes and compared in Table 7-1 below.

w = 0.555	Yeung et. al.	Klaka
7.5° Total roll moment (Nm)	0.003	0.0028
12.5° Total roll moment (Nm)	0.005	0.0049
12.5° Sway force (N)	0.121	0.093

Table 7-1: Comparison of Yeung et al. results for 2-D plate

The Yeung data was lifted from small scale graphs in the published paper and hence subject to processing errors of approximately +-15%. The close agreement on roll moment was therefore considered coincidental. The 23% difference in sway force may have been due to a combination of Reynolds number effects and the scaling assumptions used. Given that there were other differences between conditions for the two sets of experiments (plate thickness, end gap etc.) the level of agreement was considered acceptable for the purposes of validation, though questions remain regarding any direct comparison between the two data sets.

7.3   Linear and quadratic drag term

The Morison equations assumes just two components – one proportional to acceleration, the other proportional to the square of the velocity. It is possible that other terms were present; in order to investigate this a third component was added to the motion equation –linearly proportional to velocity. A typical result is shown in Figure 7-3 and Figure 7-4. The linear term showed strong dependence on angle amplitude whilst the corresponding quadratic term varied considerably with both angle amplitude and frequency, and was for the most part a negative quantity. It was difficult to reconcile these results with the rationale underlying a three-component equation so it was concluded that the addition of a linear drag term was not justified.

3-term moment model: plate 2
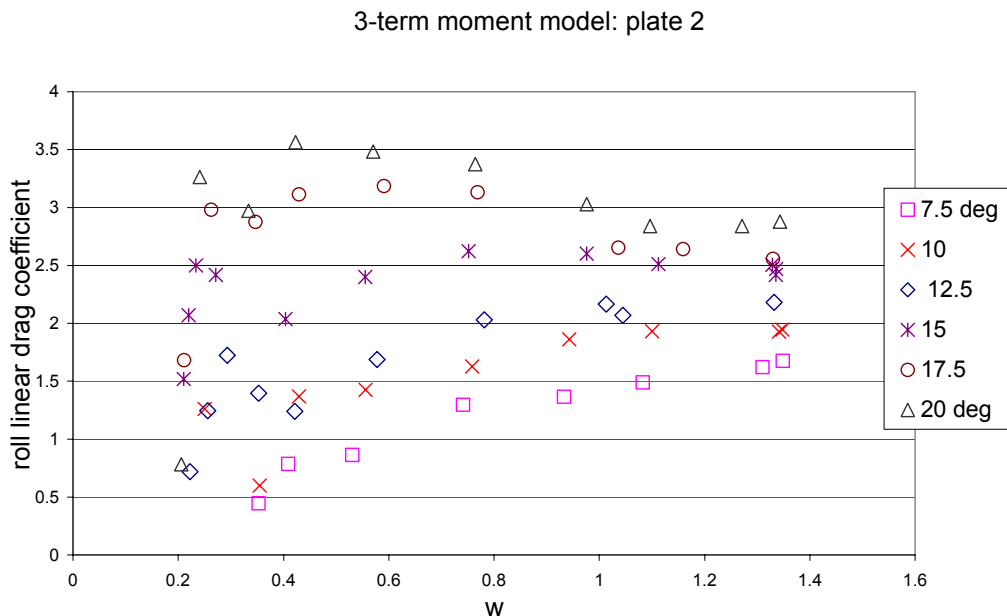
Figure 7-3 Linear drag coefficient for a 3-term model

3-term moment model: plate 2
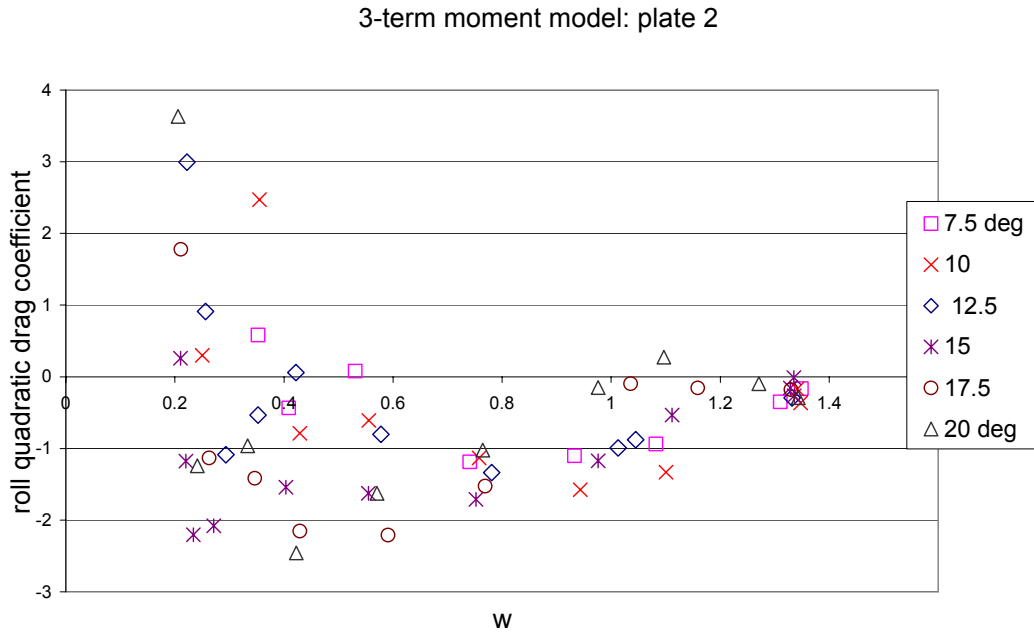
Figure 7-4 Quadratic drag coefficient for a 3-term model

7.4   Influence of oscillation frequency

For the 3-D plates the total roll moment coefficient was largely independent of oscillation frequency for most of the conditions tested i.e. the moment was proportional to the square of the velocity (Figure 7-6, Figure 7-9). This follows from the definition of the total roll moment coefficient in equation (12), repeated below:

$$C\varphi = \frac{roll\ moment}{\frac{1}{2}\rho A u^2 s}$$

The inertia coefficients for the 3-D plates were largely independent of frequency (Figure 7-12 to Figure 7-15) and the drag coefficients were only weakly related to frequency (Figure 7-16 to Figure 7-19).

The quadratic behaviour of total roll moment with respect to frequency for the 3-D plates was not exhibited by the 2-D plate (plate 1) (Figure 7-5, Figure 7-10). Here there was considerable structure in the relationship, with a transitional zone at a frequency of 2 Hz (w = 0.8) indicated. Both the inertia and drag coefficients for the 2-D plate (Figure 7-12, Figure 7-16) also showed this transitional phase. Possible explanations for the phenomenon include:

- A mechanical resonance in the rig. This would explain why the effect occurred at the same driving frequency for all angle amplitudes. However, there is no discernible energy at this frequency for tests conducted on this plate at other driving frequencies.

- A transition between two flow regimes. Transitional flows are to be found in other hydrodynamic scenarios such as the flow along a flat plate changing from laminar to turbulent boundary layer, or the onset of ventilation in a surface-piercing foil. The poor repeatability of results in this transition region was indicative of a transitional phenomenon. Yeung and others have discovered that two types of vortex shedding may exist for a 2-D oscillating plate – symmetric and asymmetric – depending on the speed of movement of the plate through the water. Flow visualisation would prove this hypothesis.

The unusual nature of these 2-D plate results, whilst interesting, was not pursued further because it was not applicable to the problem being addressed – that of a 3-D yacht appendage.

The phase angle behaviour for plate 2 is shown in Figure 7-11. The phase angle ranged from 120° to 180°, verifying that the hydrodynamic force comprises components in phase with velocity (drag) and in phase with acceleration (inertial).
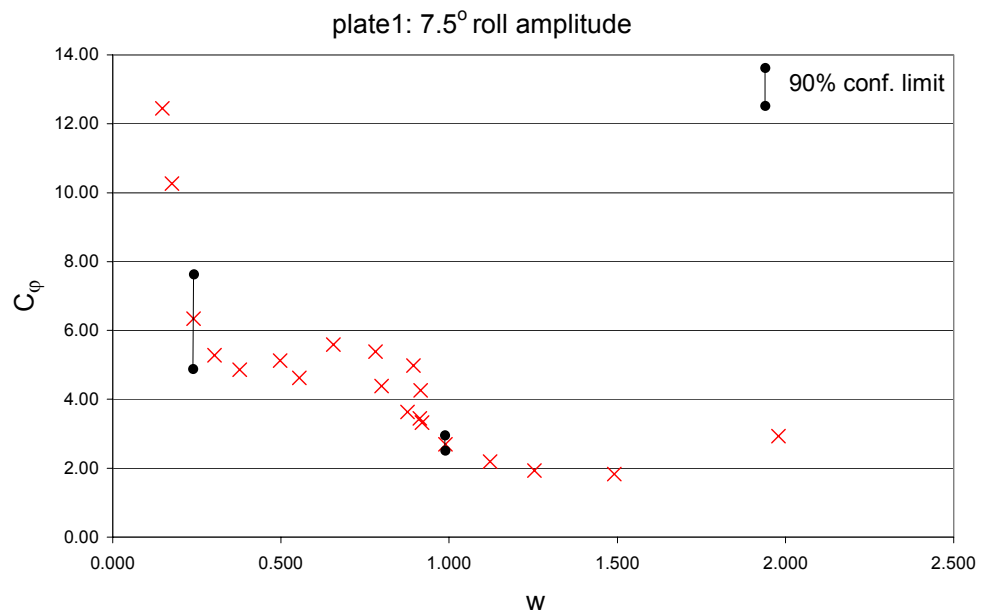
Figure 7-5 Total roll moment coefficient v. dimensionless frequency, plate 1
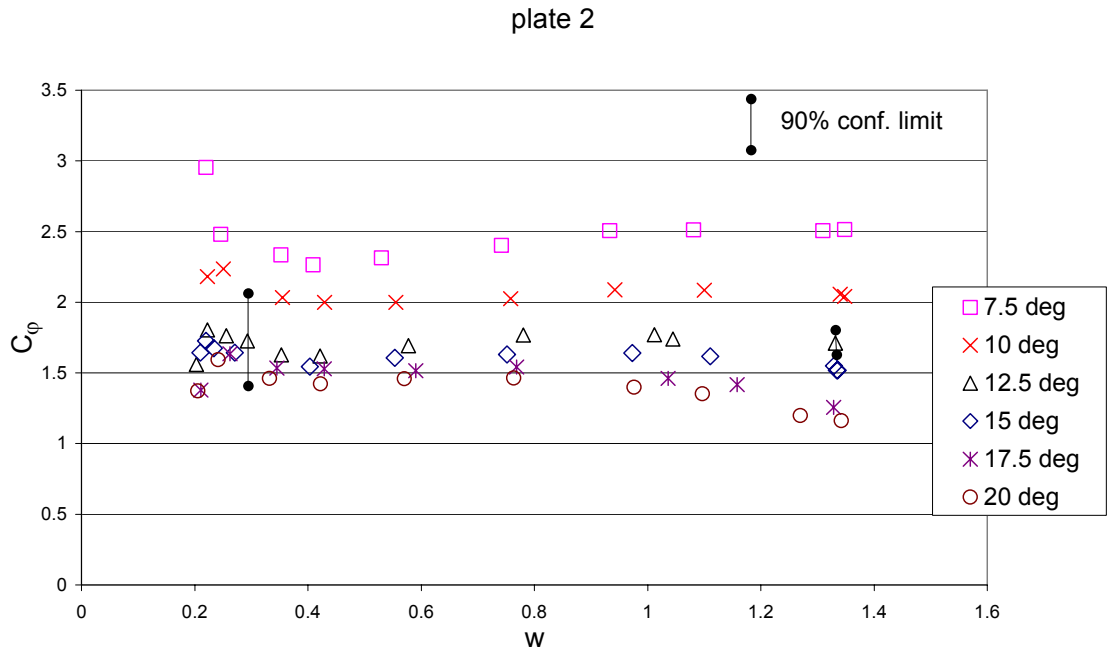
plate 2

Figure 7-6 Total roll moment coefficient v. dimensionless frequency, plate 2

plate 3: 27% ukc
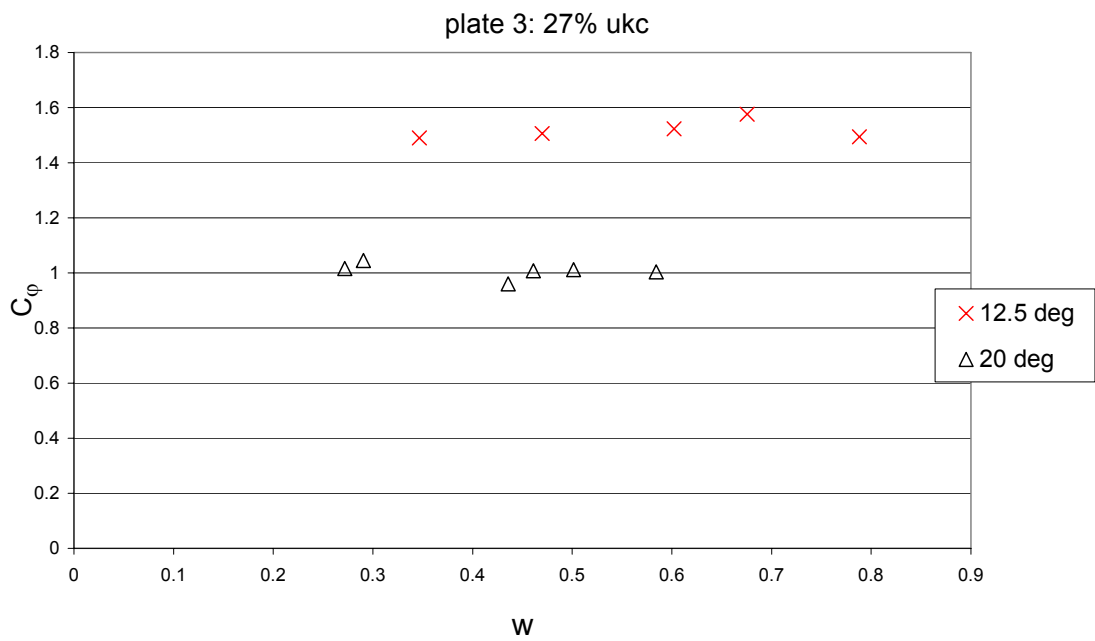
Figure 7-7 Total roll moment coefficient v. dimensionless frequency, plate 3

plate 4: 27% ukc
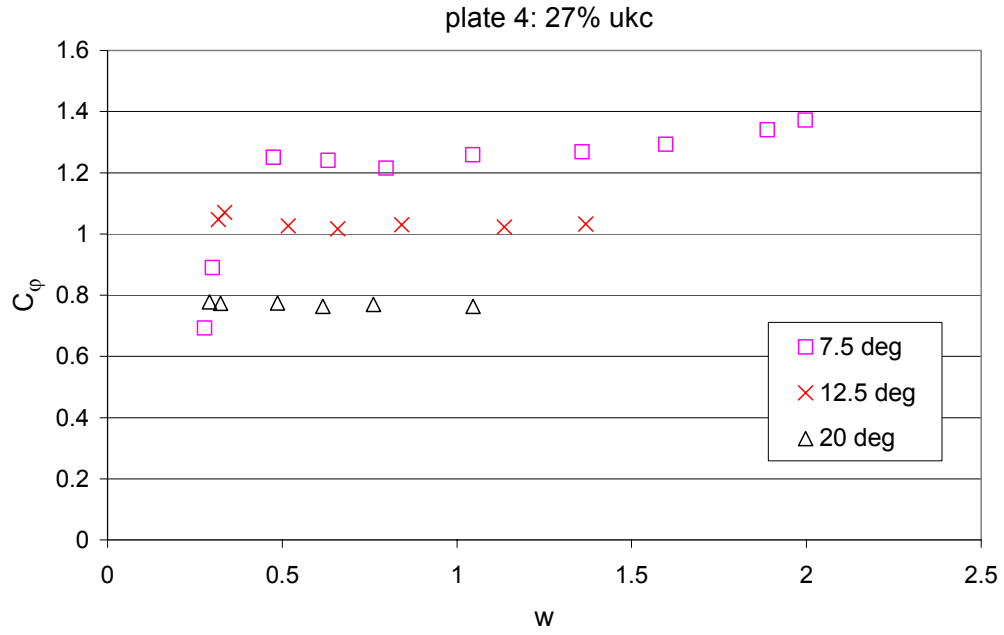
Figure 7-8 Total roll moment coefficient v. dimensionless frequency, plate 4
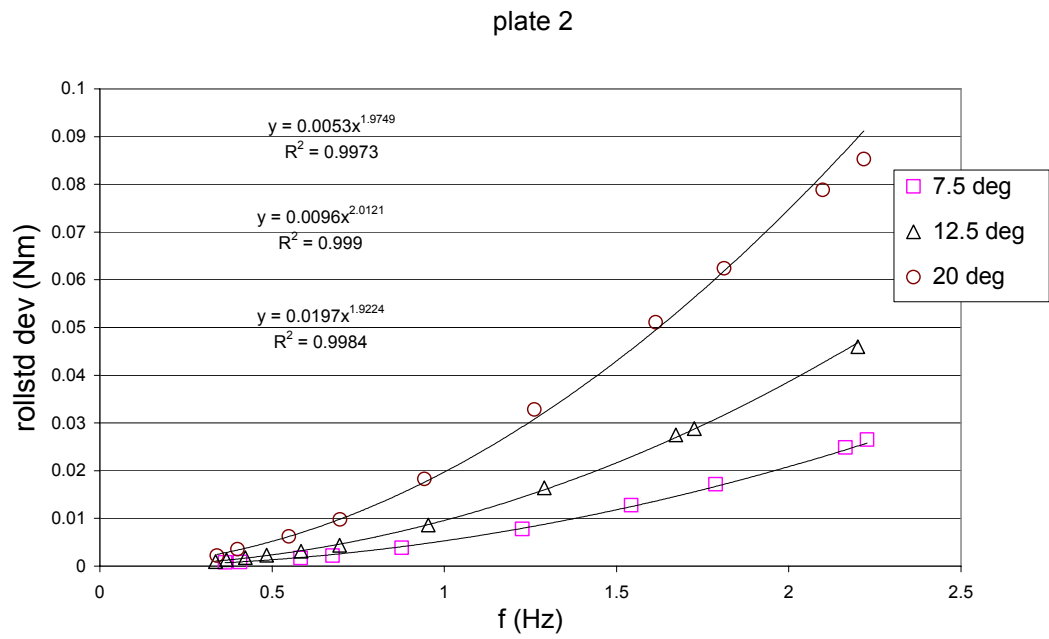
plate 2

Figure 7-9 Total roll moment v. frequency, plate 2
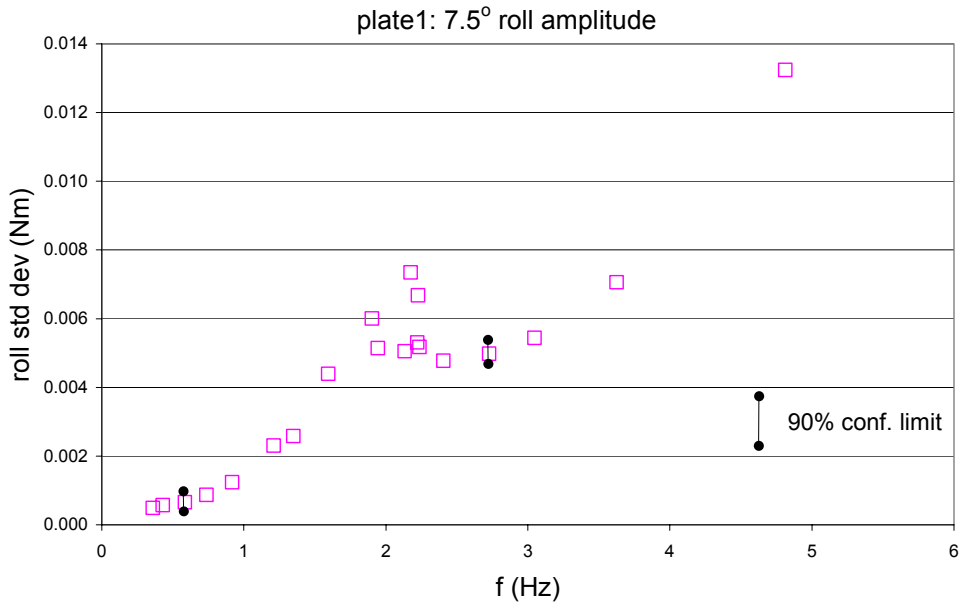
Figure 7-10 Total roll moment v. frequency, plate 1
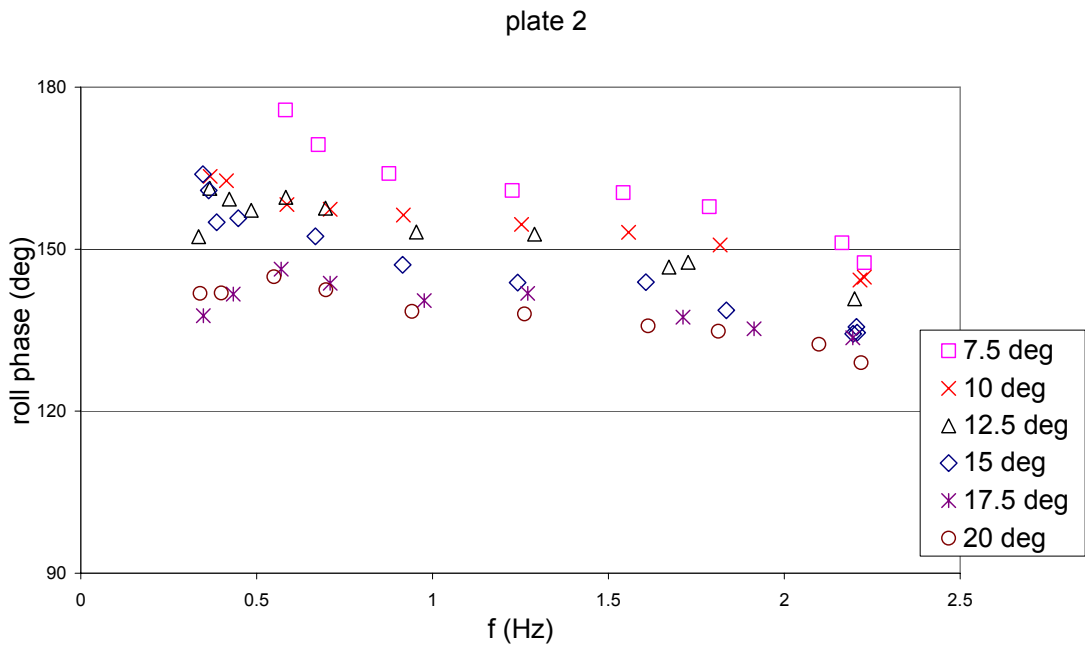
Figure 7-11 Total roll moment phase v. frequency, plate 2

roll: plate 1
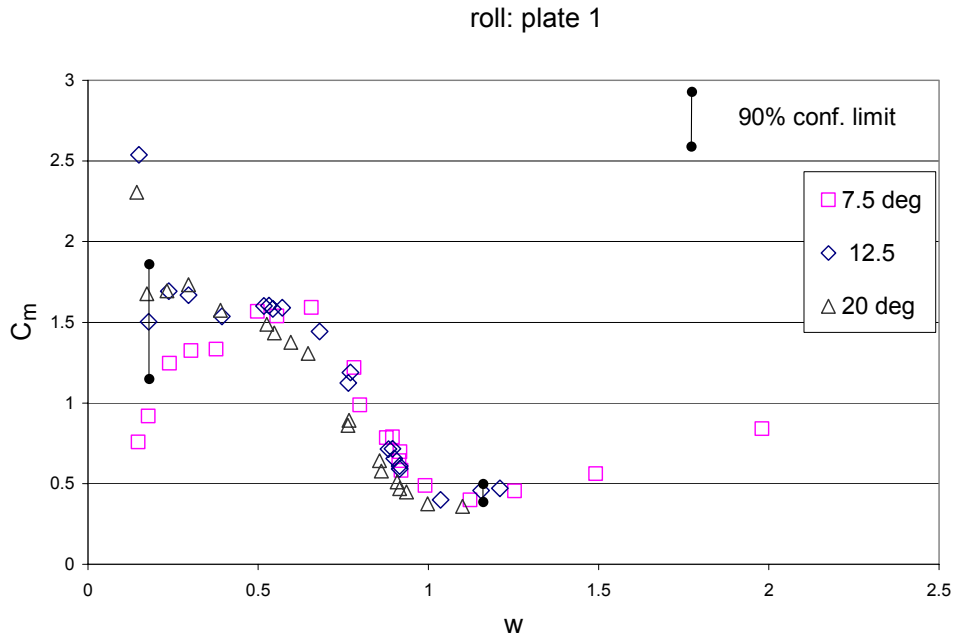
Figure 7-12 Roll inertia coefficient v. dimensionless frequency, plate 1
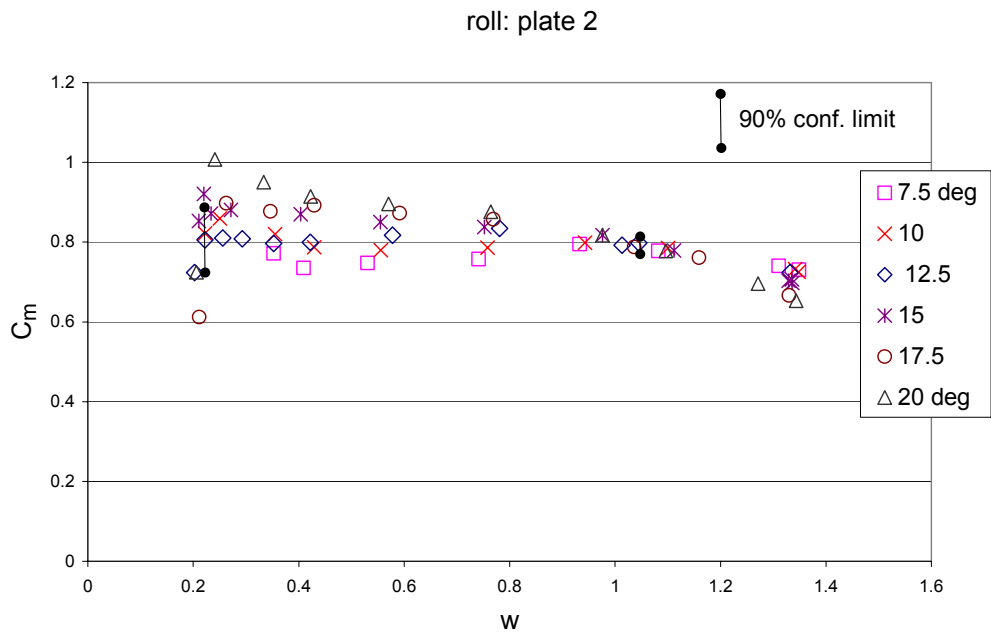
roll: plate 2

Figure 7-13 Roll inertia coefficient v. dimensionless frequency, plate 2
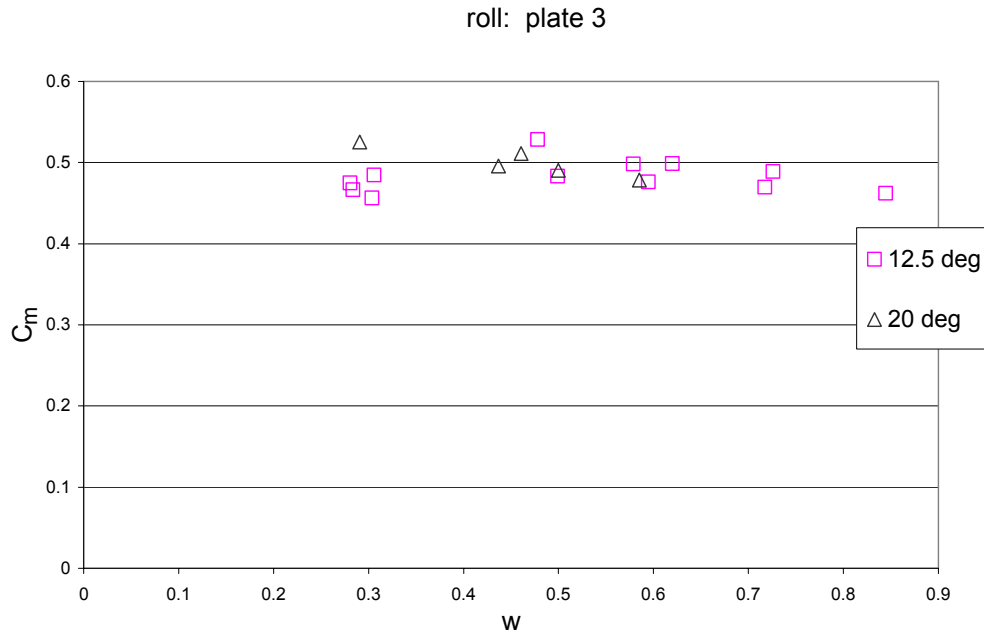
roll: plate 3

Figure 7-14 Roll inertia coefficient v. dimensionless frequency, plate 3
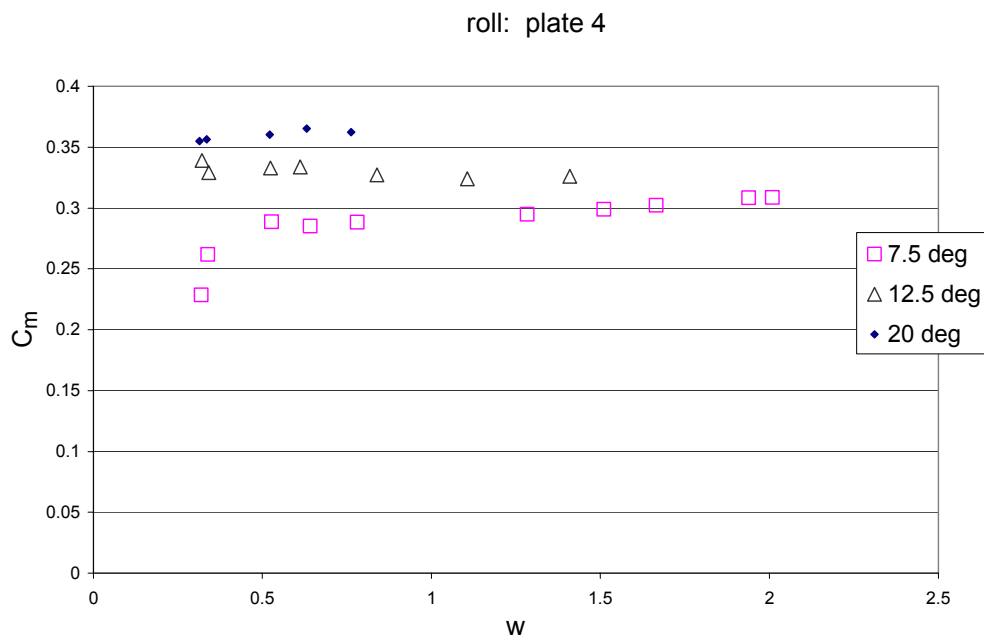
roll: plate 4

Figure 7-15 Roll inertia coefficient v. dimensionless frequency, plate 4

10/07/2003
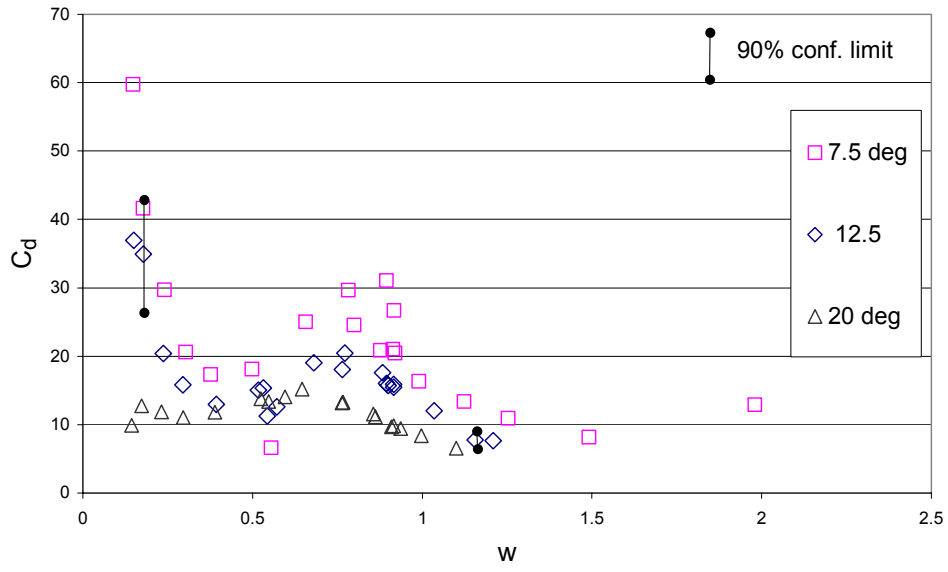
roll: plate 1

Figure 7-16 Roll drag coefficient v. dimensionless frequency, plate 1

roll: plate 2
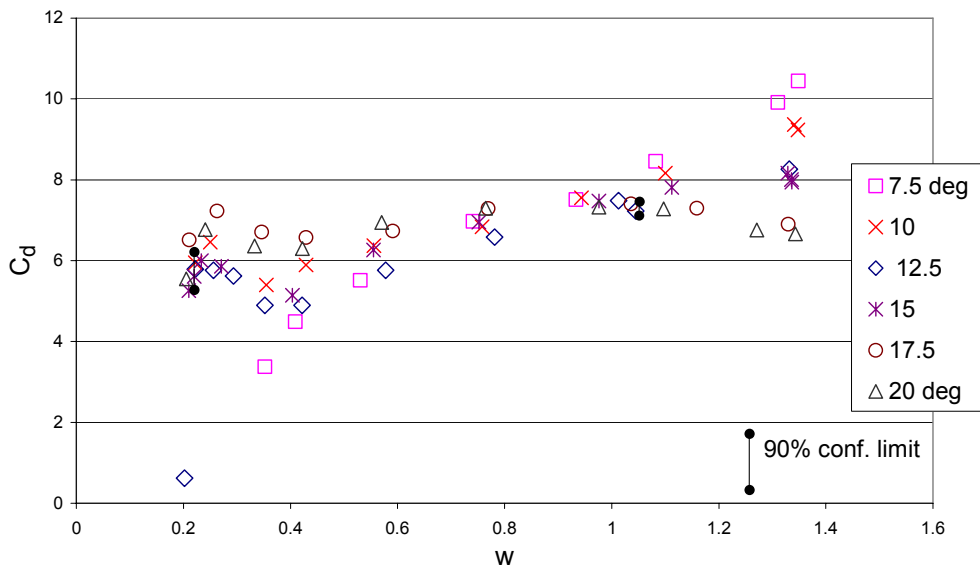
Figure 7-17 Roll drag coefficient v. dimensionless frequency, plate 2

roll: plate 3
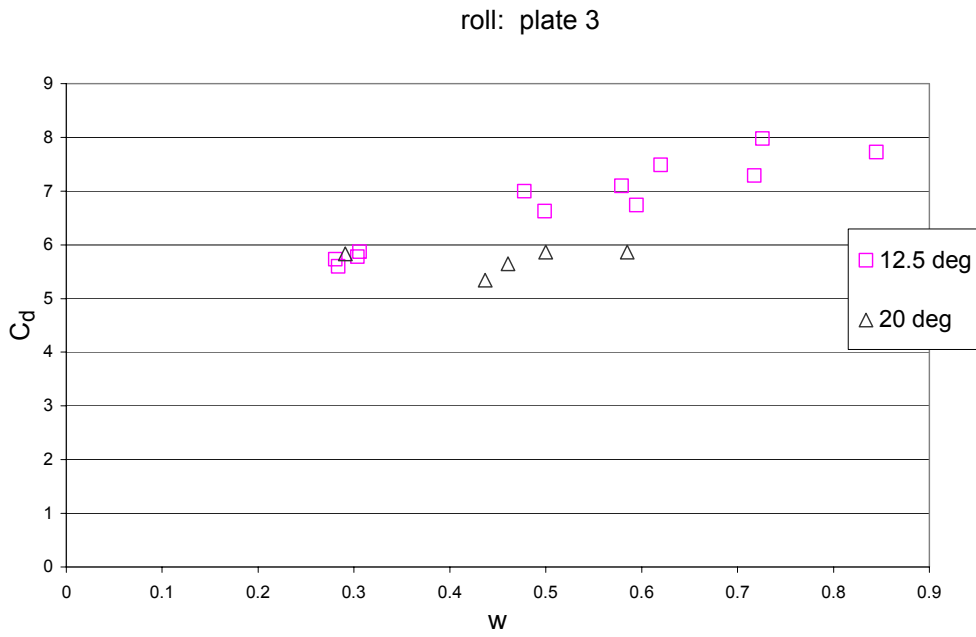
Figure 7-18 Roll drag coefficient v. dimensionless frequency, plate 3

roll: plate 4
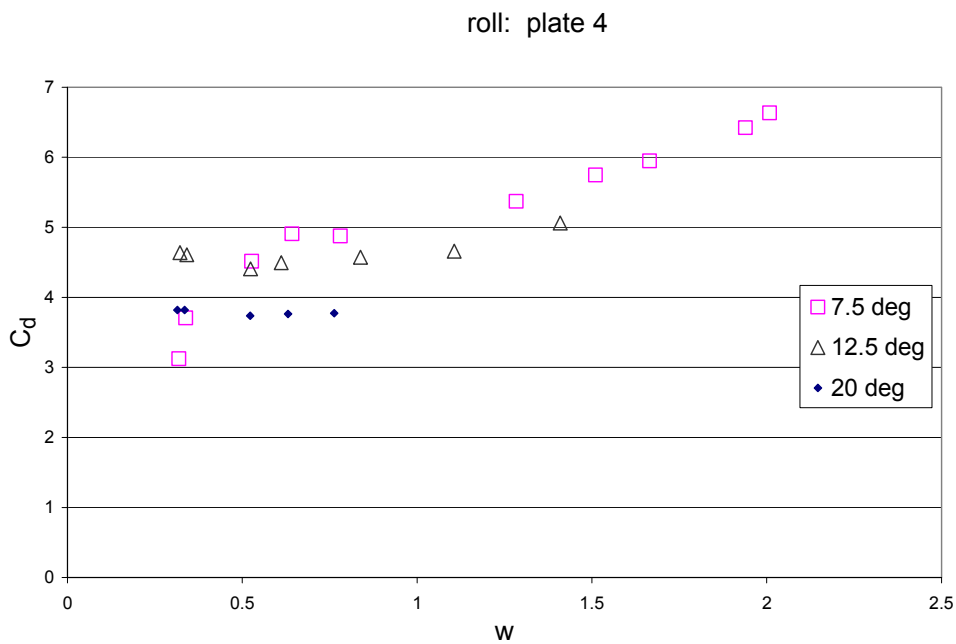
Figure 7-19 Roll drag coefficient v. dimensionless frequency, plate 4

7.5   Influence of angle amplitude

It was not considered practicable to generate cross-plots of coefficients against angle amplitude at constant frequency because it was not possible to set the motor speed at exactly repeatable values. Therefore a curve fitting procedure would have been required, which

would need to use data points weighted in relation to the varying error limits with frequency. The result would be more likely to show the effect of the chosen data processing technique used rather than any hydrodynamic phenomenon. Nevertheless the influence of angle amplitude can be discerned from Figure 7-5 to Figure 7-19. There was a general trend towards lower coefficient with increasing angle amplitude.

7.6   Effect of underplate clearance

The underplate clearance was defined as:

$$UKC = \frac{h}{s}$$ (16)

where

h = distance from the tip of the plate to the bottom of the channel

s = plate span

The UKC is usually expressed as a percentage.

The effect of underplate clearance on total roll moment for plate 4 is illustrated in Figure 7-20 . Similar trends were evident for plate 3 and for the sway force for the range of angles tested. The influence of underplate clearance on inertia and drag coefficients was also similar (Figure 7-21 and Figure 7-22). There was a very slight increase in roll moment at 2.5% UKC but no significant difference in roll moment between 15% and 27% UKC.

For application to a yacht at anchor, 2.5% clearance is unrealistic as the yacht would impact the sea bed on almost every wave. Therefore, within the context of the project aims, there was no evidence in these results to suggest that proximity to the seabed affects the roll moment. A proviso is added that the wave particle velocities in an ocean environment will be influenced by the presence of the seabed; it is the response to those particle velocities that is not affected.

There is the possibility that a plate of proportionally greater bottom edge length may exhibit some clearance effect. Further, the bottom roughness may play some part (the channel bed was a pliant coating with longitudinal grooves of approximately 0.5mm height).

Plates 1 and 2 could not be mounted low enough to conduct tests at less than 100% *UKC*, so effects of underplate clearance were not investigated for them.
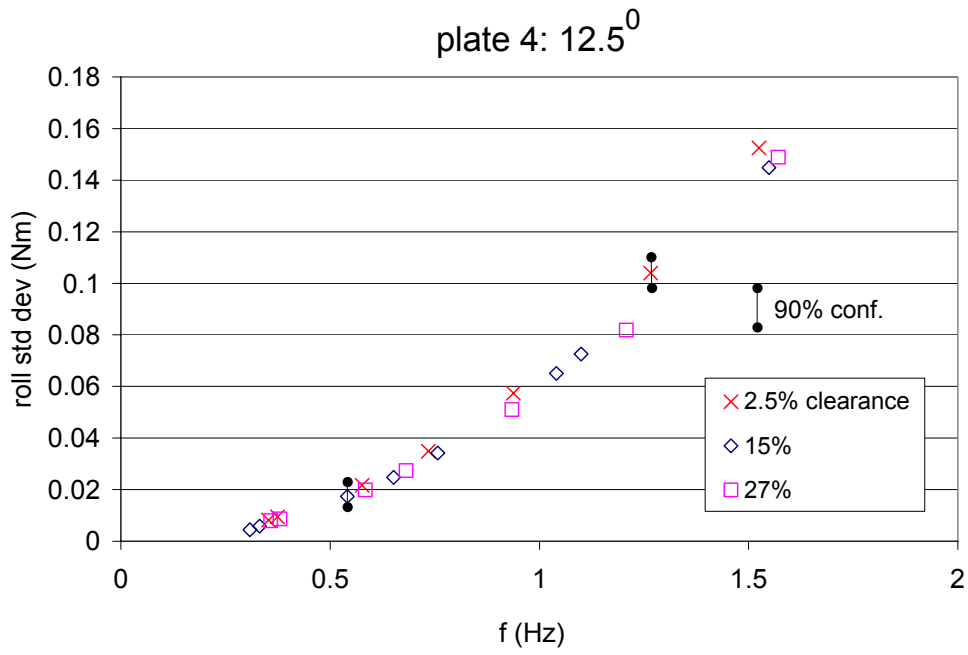
Figure 7-20 Effect of under-plate clearance on total roll moment
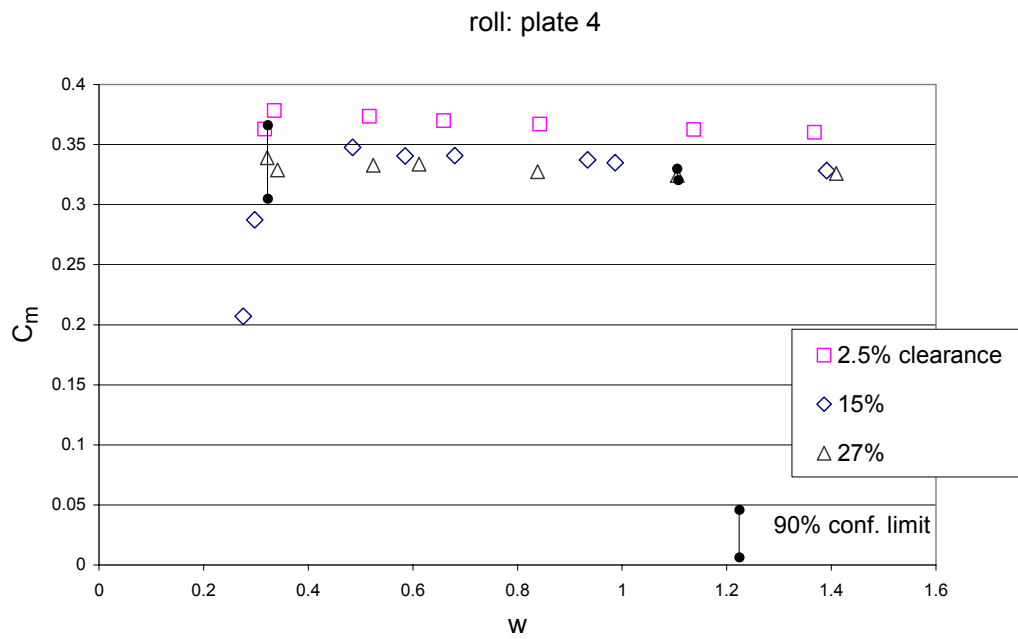
Figure 7-21 Effect of under-plate clearance on roll inertia coefficient

roll: plate 4
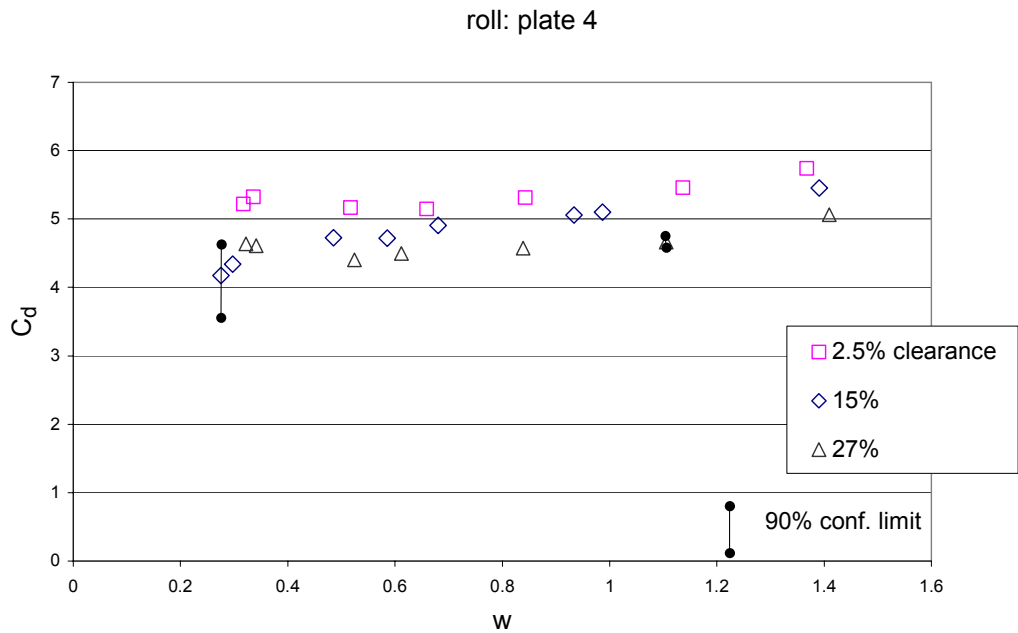
Figure 7-22 Effect of under-plate clearance on roll drag coefficient

7.7 Effect of plate shape

The total roll moment coefficient showed no immediately apparent relationship to plate geometry (Figure 7-23). The following model yielded an engineering approximation for much of the data:

$$C_\varphi = 5.5 AR^{-0.5} \varphi^{-0.5} \qquad (17)$$

where:

$C\varphi$ = total roll moment coefficient

AR = aspect ratio

φ= angle amplitude (deg)

This model is compared with the experimental data in Figure 7-24, Figure 7-25 and Figure 7-26.

The inertia coefficient for the 3-D plates did not exhibit any straightforward relationship with plate geometry either (Figure 7-27). However, the relationship

$$C_m = 0.4(AR)^{-0.5}\left(\varphi^{0.25}\right) \qquad (18)$$

was a reasonable approximation (Figure 7-28, Figure 7-29 and Figure 7-30)

The drag coefficient was less consistent in its behaviour (Figure 7-31), but followed an approximate relationship, illustrated in Figure 7-32, Figure 7-33 and Figure 7-34:

$$C_d = 6AR^{-0.5} + 10w\varphi^{-1} \qquad\qquad (19)$$

where:

w = dimensionless frequency

AR = aspect ratio

φ = roll angle amplitude (deg)

All aspect ratio dependency in all three models follows a pattern found in many aspects of aerodynamics and hydrodynamics theory (Glauert, 1959), (Milne-Thomson, 1968).
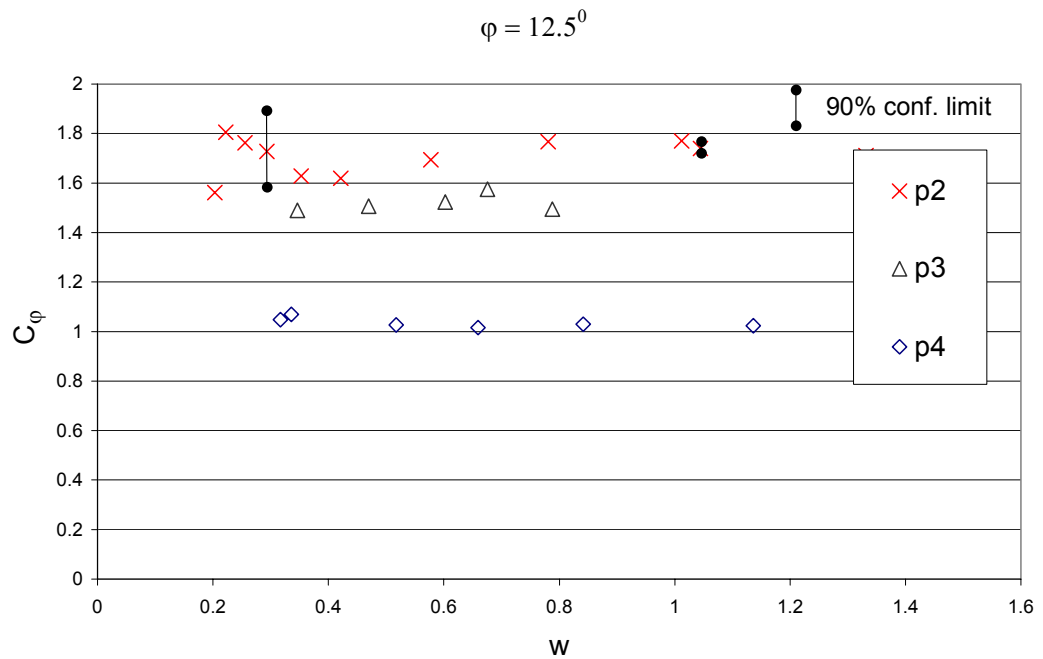
Figure 7-23 Total roll moment coefficient at 12.5° amplitude

$\varphi = 7.5^0$
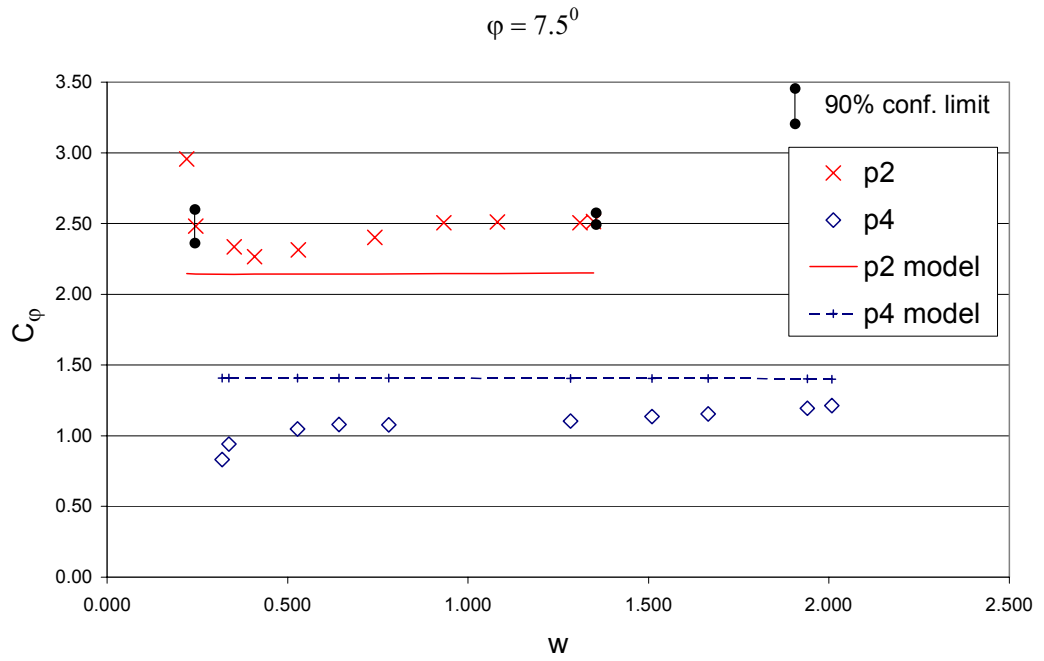
Figure 7-24 Effect of plate geometry on total roll moment coefficient, 7.5° amplitude

$\varphi = 12.5^0$
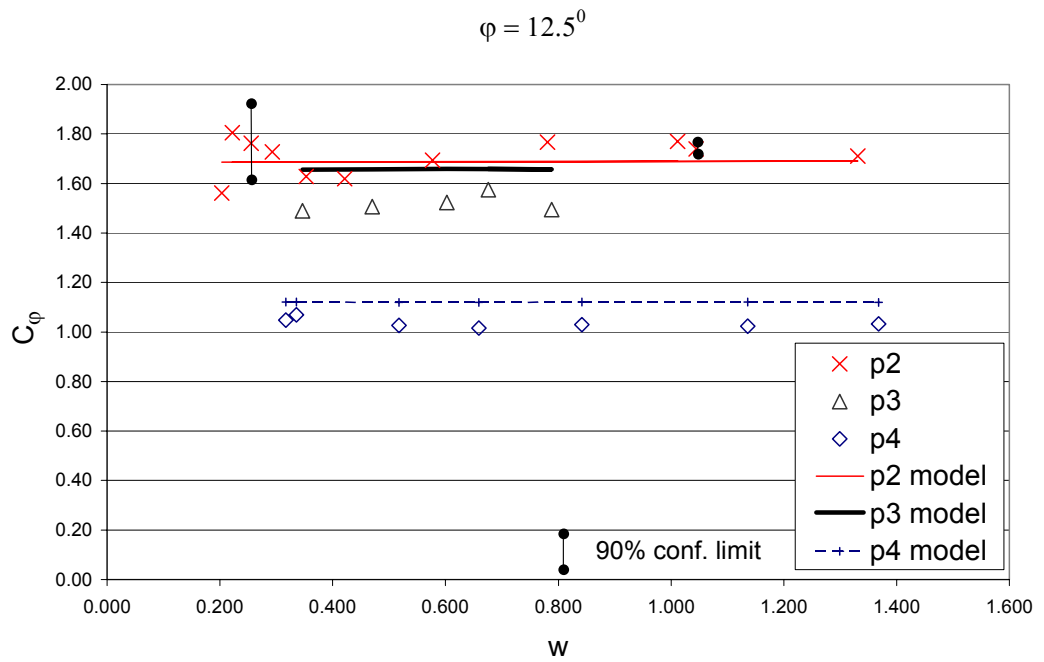
Figure 7-25 Effect of plate geometry on total roll moment coefficient , 12.5^0 amplitude

$$\varphi = 20^0$$
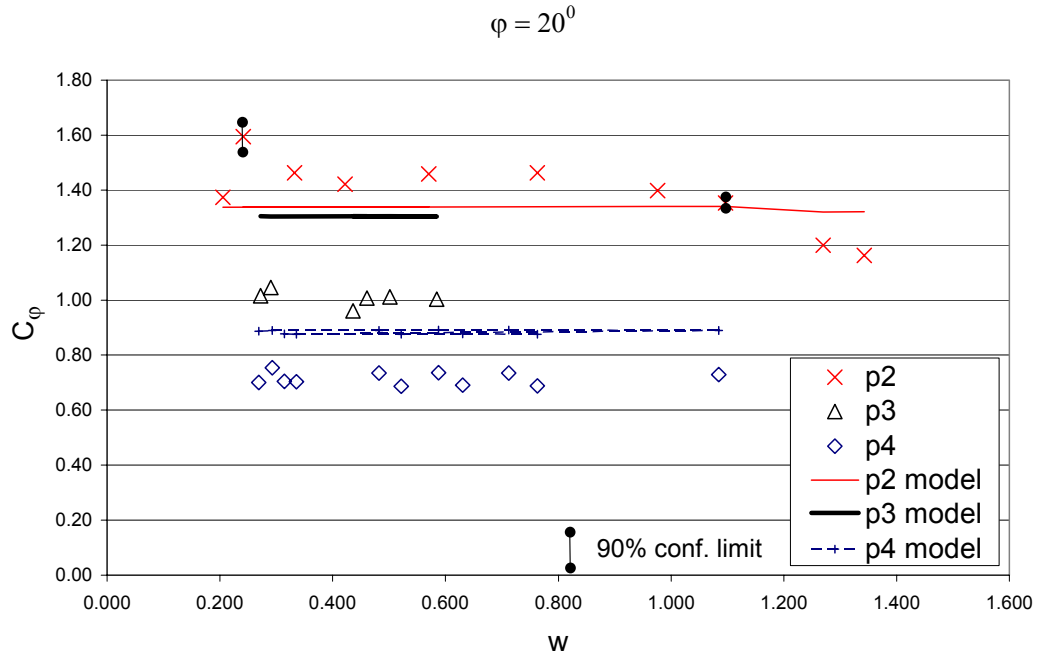
Figure 7-26 Effect of plate geometry on total roll moment coefficient , 20^0 amplitude
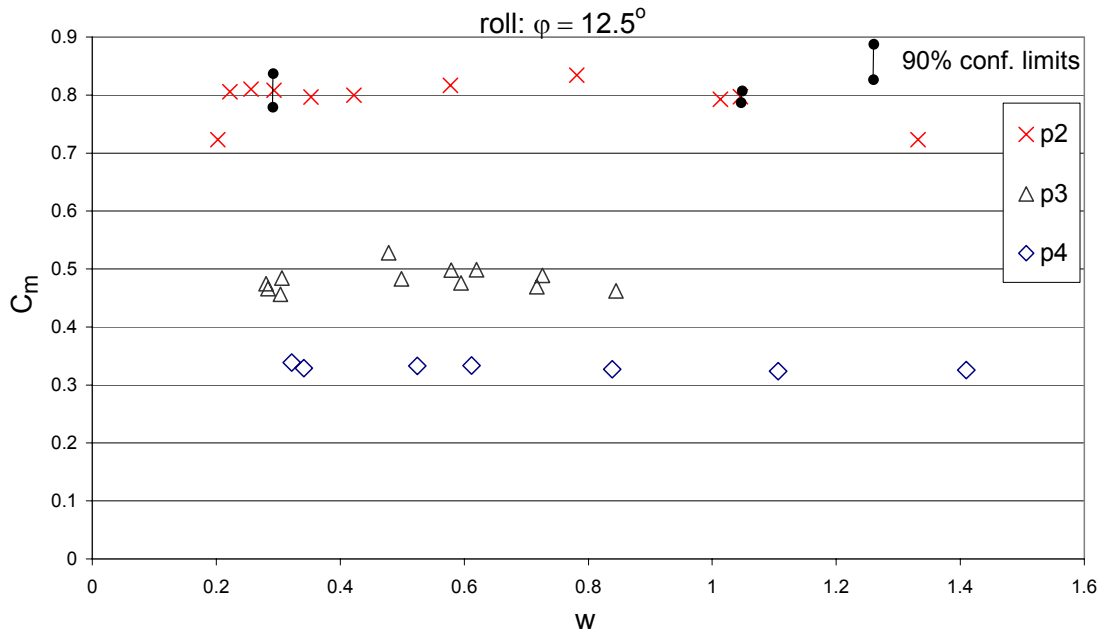
Figure 7-27 Roll inertia coefficient at 12.5° amplitude
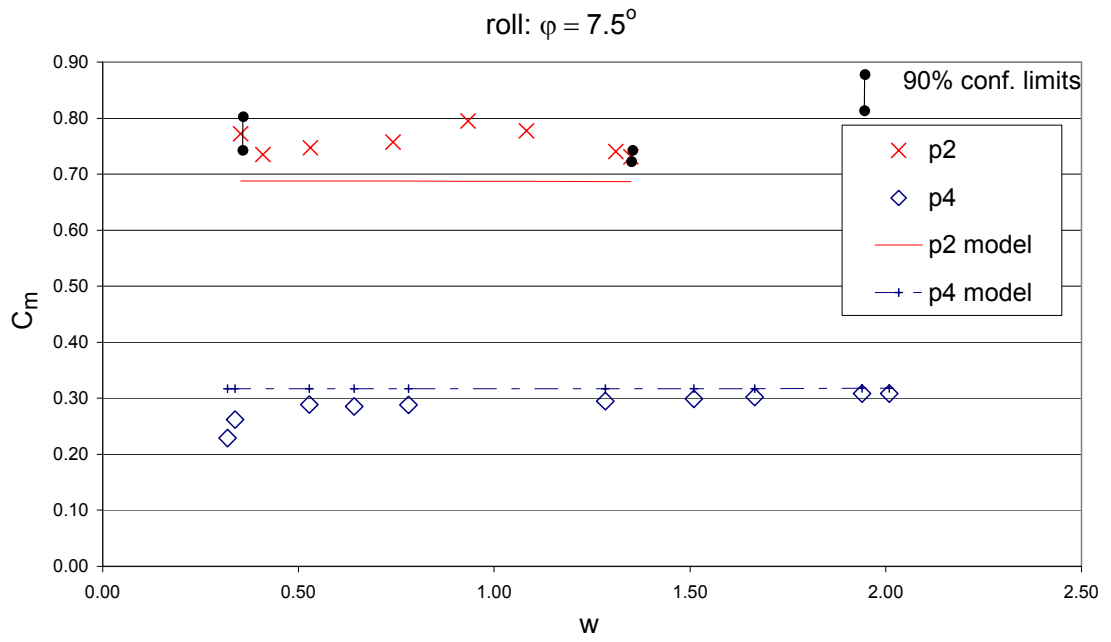
Figure 7-28 Effect of plate geometry on roll inertia coefficient, 7.5[0] amplitude
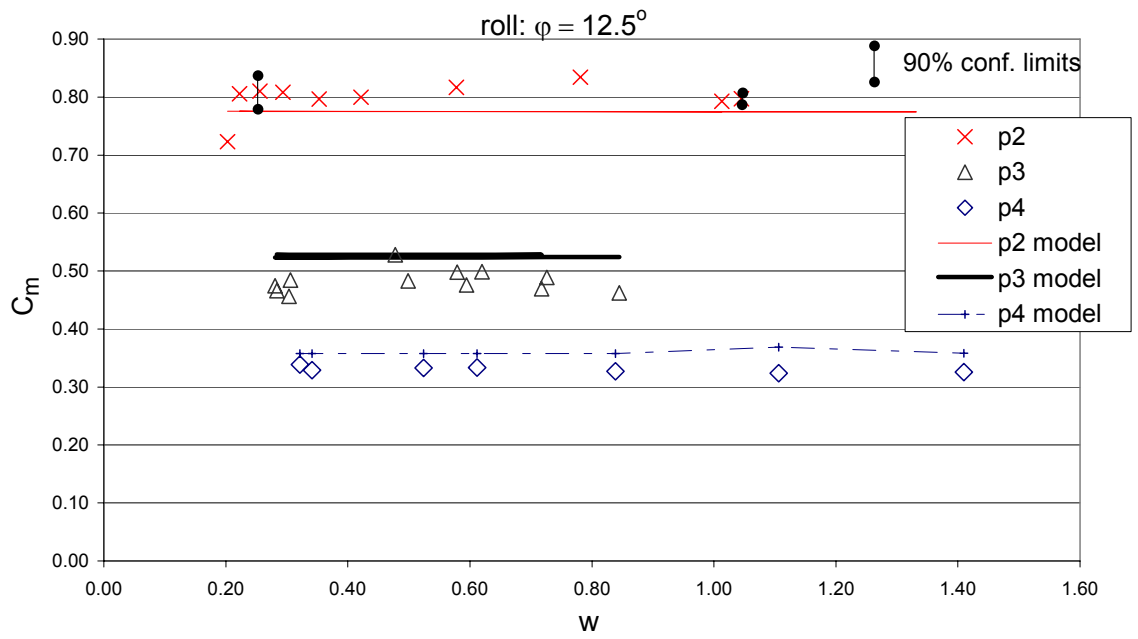
Figure 7-29 Effect of plate geometry on roll inertia coefficient, 12.5[0] amplitude
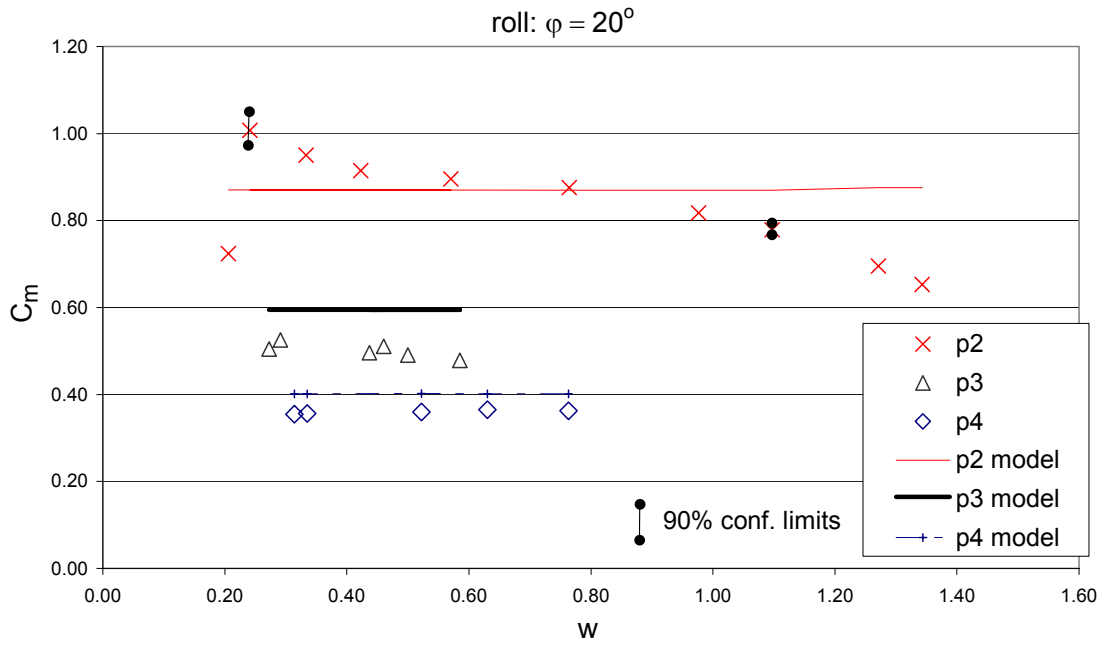
Figure 7-30 Effect of plate geometry on roll inertia coefficient, 20^0 amplitude
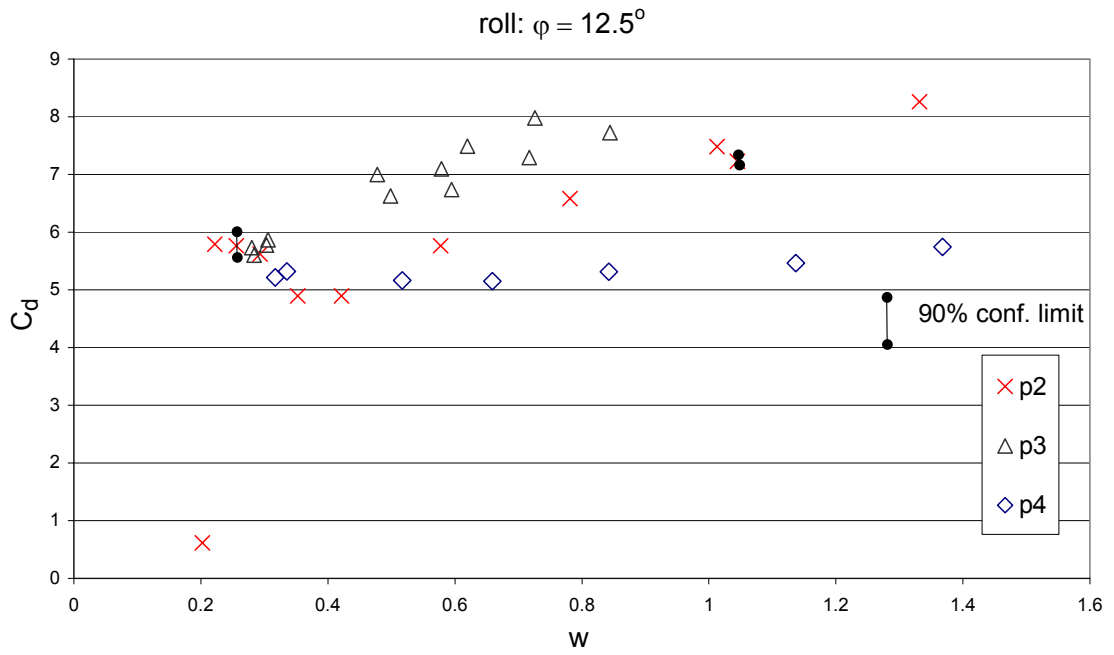
Figure 7-31 Roll drag coefficient at 12.5° amplitude

roll: φ = 7.5⁰
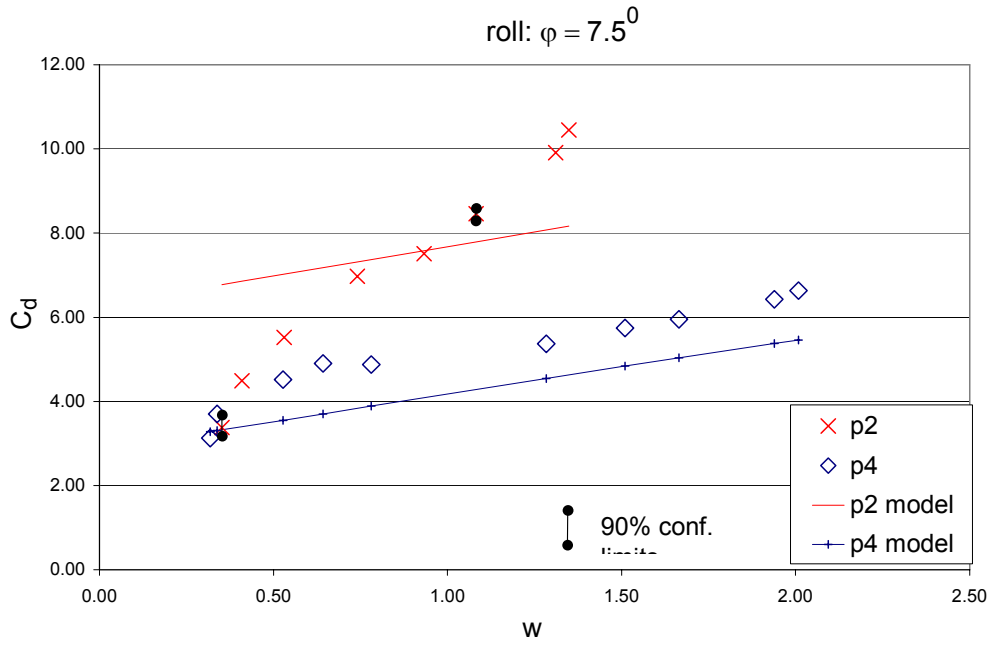
Figure 7-32 Effect of plate geometry on roll drag coefficient, 7.5⁰ amplitude

roll: φ = 12.5⁰

Figure 7-33 Effect of plate geometry on roll drag coefficient, 12.5⁰ amplitude
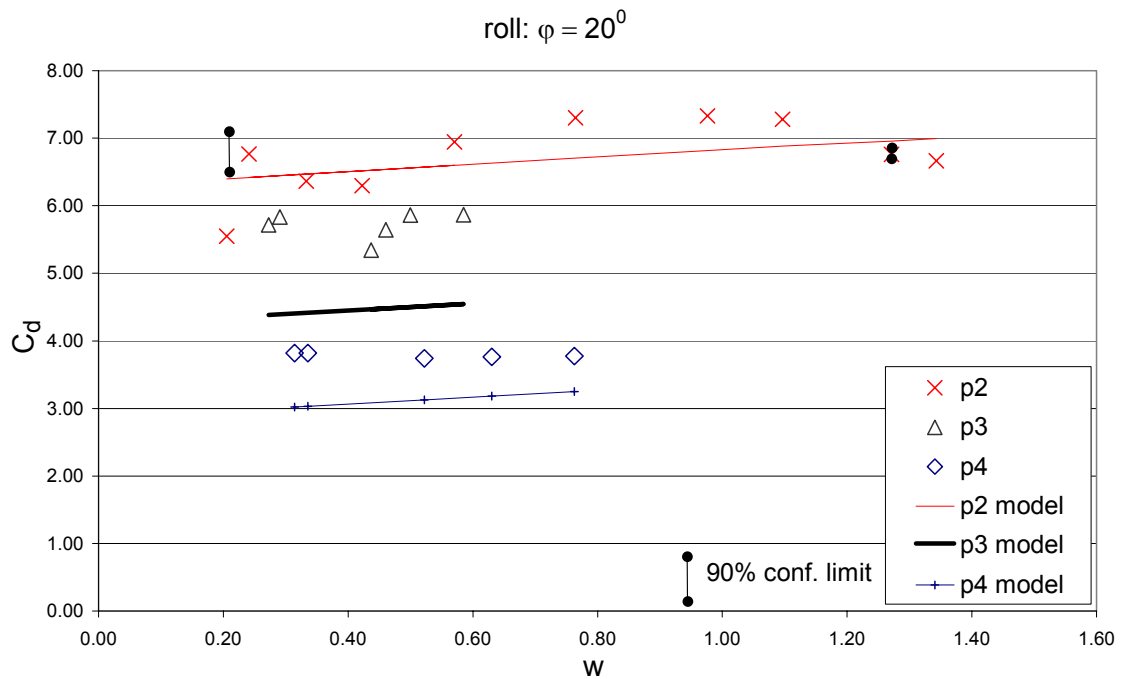
Figure 7-34 Effect of plate geometry on roll drag coefficient, 20^0 amplitude

7.8   Centre of pressure

The spanwise centre of pressure is the point at which the sway force may be considered to act – a concept similar to that of a centre of gravity. It was determined by dividing the standard deviation of the roll moment signal by that of the sway force signal. It was found to lie between 50% and 80% of span for most conditions tested (Figure 7-35). The centre of pressure time series was found by dividing the roll moment signal by the sway force signal at each time step. A typical result is shown in Figure 7-36, from which it is evident that the centre of pressure did not vary substantially within an oscillation. The instances within the oscillation when the sway force was very small resulted in the centre of pressure calculation being dominated by experimental error. Consequently the data at those instances has been omitted from the figure.

The centre of pressure for a plate in steady uniform flow without end effects would be expected to be located at 50% of the span. The plates in these experiments underwent sinusoidal oscillation, generating an instantaneous velocity distribution that increased approximately linearly along the span. If the forces were proportional to velocity squared – a reasonable assumption for steady flow – this would result in a centre of pressure at 67% of the span. However, for an oscillating plate the forces are dependent on both velocity and acceleration, so the steady flow approximation is a poor one.

$\varphi = 12.5^o$
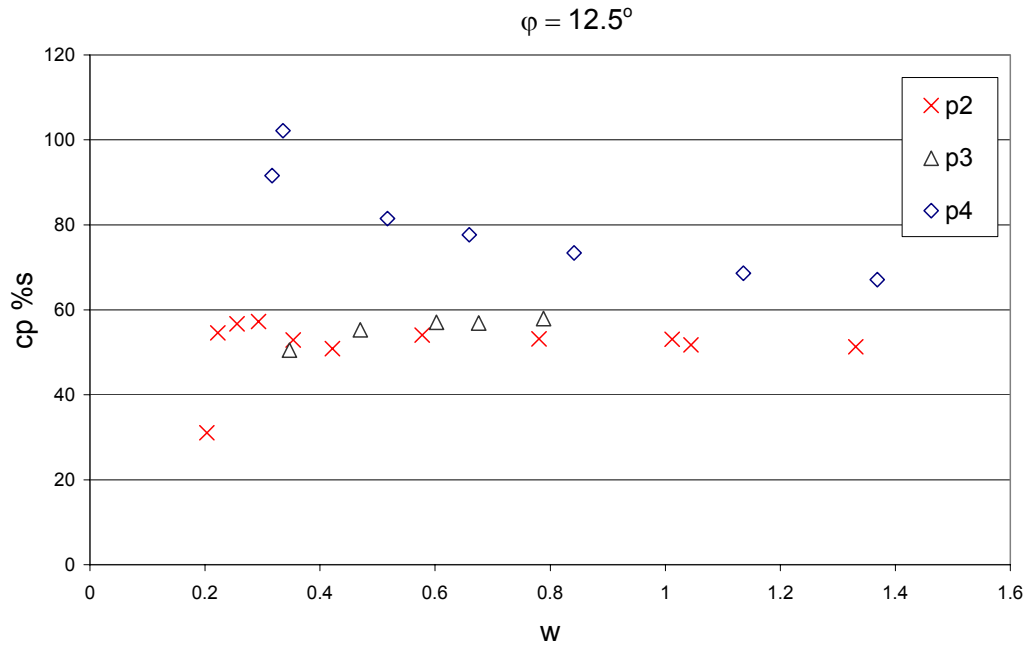
Figure 7-35 Effect of plate geometry on centre of pressure

run 152
plate 2   1.9Hz   17.5^o
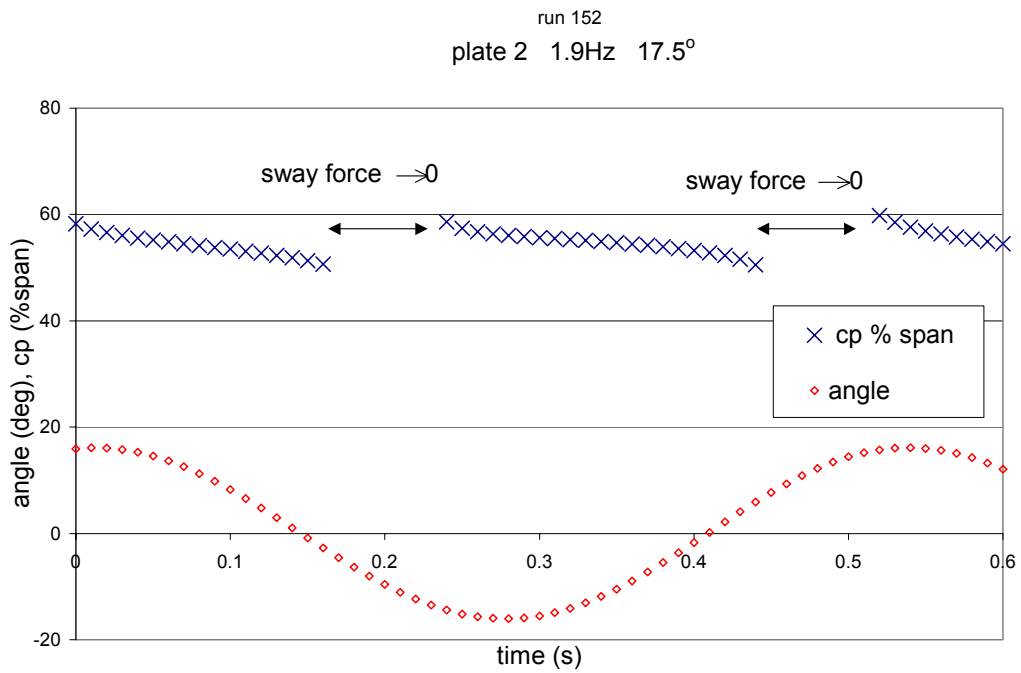
Figure 7-36 Centre of pressure v. time

7.9   **Heave force**

The errors in the heave force measurements were an order of magnitude greater than in the sway and roll measurements, owing to the very low strains induced (see 6.1). However, the heave force contributed only about 15% of the total hydrodynamic force. It did not influence the roll moment measurement at all because this was determined directly from the crank attachment strain gauges, with no need to refer to the hinge support gauges. The hypothesis that the total hydrodynamic force was normal to the plate was tested by comparing the heave force predicted from the sway force using this hypothesis, with the measured heave. The results (Figure 7-37) show that, aside from an unaccountable offset, the total force was normal to the plate, within the limits of the large experimental error in these measurements.
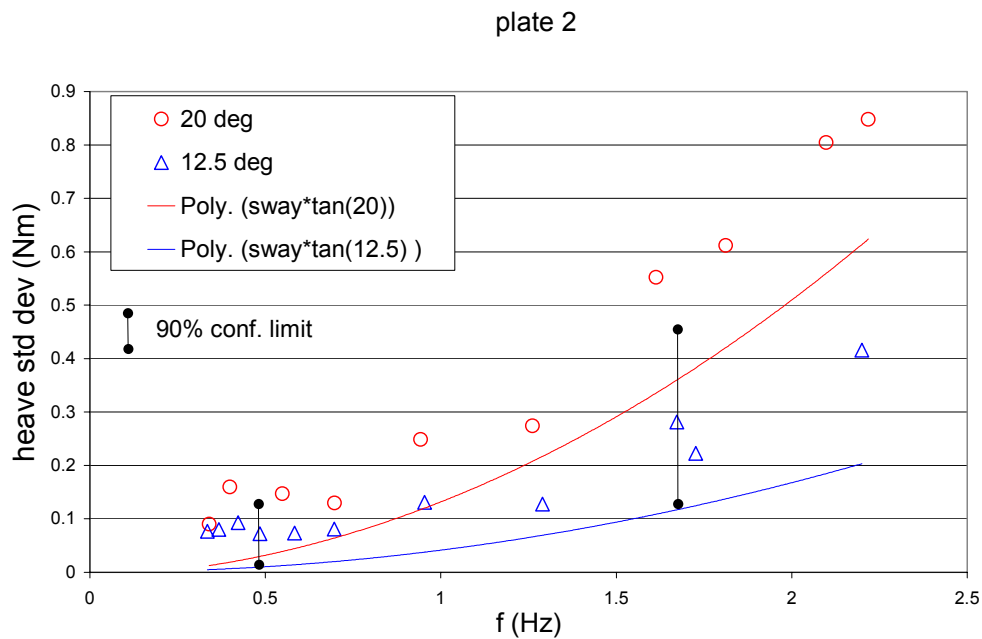
Figure 7-37 Heave force normalcy test

8   CONCLUSIONS

For the conditions of the experiment and within the limits of experimental error, the following conclusions are drawn:

- the 2-D case is not representative of 3-D flow conditions.

- under keel clearance has no practical influence for yacht keels.

- the total roll moment, roll inertia, roll drag and sway force coefficients show a very weak dependency on oscillation frequency and angle amplitude.

- the total roll moment coefficient for the 3-D plates is approximately proportional to the inverse square root of the chord.

- The roll inertia coefficient of the 3-D plates is approximately proportional to the inverse square root of the geometric aspect ratio.

- The roll quadratic drag coefficient of the 3-D plates is approximately proportional to (sqrt(area)/perimeter)$^{1.5}$

- There is no justification for including a third (linear) term in the equation of motion for the plates.

- There is a possible region of transitional flow for the 2-D plate, not evidenced in the results for the 3-D plates.

- the hydrodynamic force acts normal to the plate surface.

9   RECOMMENDATIONS FOR FURTHER WORK

9.1   Incorporation of results into time simulation program

The force and moment time series should be incorporated into the time simulation program written by the author (Klaka, 2001b). The program divides the plate into spanwise strips then calculates the Morison coefficients for the conditions of each strip. It is proposed to modify this approach by calculating the Morison coefficients of the entire plate in accordance with the parameter dependencies identified from the current work.

9.2   Flow visualisation

Flow visualisation is recommended in order to determine whether the 2-D plate undergoes a transitional phase as indicated in the results. Visualisation of the 3-D plate flow might provide further insight to the importance of chord length and seeming unimportance of underplate clearance

9.3   Further measurements

Extension of the data sets for the 3-D plates to higher frequencies is required to determine whether the transition characteristics of 2-D flow are present in 3-D. This would require upgrading the hinge supports and crank attachment in order to avoid breakdown of the glue join between the gauges and the substrate.

There may be some benefit in conducting the tests for plate 2 at low underplate clearances, to see if and how plate shape plays a role in clearance effects. This would require modification of the rig to increase the range of vertical movement of the lower support plate, or placing an infill on the channel bed.

The effect of channel bed roughness on underplate clearance effects could be investigated.

Plates of different thickness, planform and edge shape could be investigated in order to determine the effects these parameters have, if any.

The blockage correction for large objects in separated flow with a free surface requires investigation in order to enable better comparison with results from other experiments.

10 REFERENCES

Bearman, P. W., Downie, M. J., Graham, M. R. and Obasaju, E. D. (1985) Forces on cylinders in viscous oscillatory flow at low Keulegan-Carpenter numbers *Journal of Fluid Mechanics,* **154,** 337-356.

Bertram, V. (2000) *Practical ship hydrodynamics,* Butterworth-Heinemann, Oxford, UK.

Chakrabarti, S. K. (1987) *Hydrodynamics of offshore structures,* Computational Mechanics, Southampton.

Glauert, H. (1959) *The elements of aerofoil and airscrew theory,* Cambridge University Press, Cambridge.

Harvald, S. A. (1983) *Resistance and propulsion of ships,* Wiley, New York.

IOtech (2000) *DaqBook Series*, 9 July 2003, http://www.iotech.com/catalog/daq

Johnson, B. (1999) ITTC symbols and terminology list**,** U.S. Naval Academy.

Keulegan, G. H. and Carpenter, L. H. (1958) Forces on cylinders and plates in an oscillating fluid *Journal of Research of the National Bureau of Standards,* **60,** 423-440.

Kinney, F. S. (1973) *Skene's elements of yacht design,* A & C Black, London.

Klaka, K. (2000) Response of a vessel to waves at zero ship speed: preliminary full scale experiments**,** *CMST 2000-21* Centre for Marine Science & Technology, Curtin University 28.

Klaka, K. (2001a) Model tests on a circular cylinder with appendages**,** *CMST 2001-14* Centre for Marine Science & Technology, Curtin University of Technology 26.

Klaka, K. (2001b) A simplified roll model**,** *CMST 2001-09* Centre for Marine Science & Technology, Curtin University of Technology 21.

Larsson, L. and Eliasson, R. E. (1994) *Principles of yacht design,* International Marine, Camden USA.

Lewis, E. V. (1989) *Principles of Naval Architecture,* Society of Naval Architects and Marine Engineers, Jersey City.

Lloyd, A. (1989) *Seakeeping: ship behaviour in rough weather,* Ellis Horwood, Chichester.

Milne-Thomson, L. M. (1968) *Theoretical hydrodynamics,* Dover, New York.

Pankhurst, R. C. and Holder, D. W. (1965) *Wind-tunnel technique,* Pitman, London.

Rae, W. H. and Pope, A. (1984) *Low-speed wind tunnel testing,* John Wiley & Sons.

Ridjanovic, M. (1962) Drag coefficients of flat plates oscillating normally to their planes *Schiffsteknik,* **45,** 13-17.

Sarpkaya, T. and O'Keefe, J. L. (1995) Oscillating flow about two- and three-dimensional bilge keels In *14th International Conference on Offshore Mechanics and Arctic Engineering*, Vol. 1-A American Society of Mechanical Engineers, Copenhagen, pp. 263-270.

Scott, J. R. (1966) A blockage corrector *Transactions Royal Institution of Naval Architects,* **108,** 153-163.

Scott, J. R. (1976) Blockage correction at sub-critical speeds *Transactions Royal Institution of Naval Architects,* **118,** 169-179.

Yeung, R., Cermelli, C. and Liao, S. W. (1997) Vorticity fields due to rolling bodies in a free surface - experiment and theory In *21st Symposium on Naval Hydrodynamics*National Academy Press, Trondheim, Norway, pp. 359-376.

Yeung, R. W. and Cermelli, C. A. (1998) In *Advances in Fluid Mechanics*, Vol. 16 (Ed, Tyvand, P.) Computational Mechanics, Southampton, UK, pp. 35.

Yeung, R. W., Liao, S.-W. and Roddier, D. (1998) Hydrodynamic coefficients of rolling rectangular cylinders *International Journal of Offshore and Polar Engineering,* **8,** 241-250.

LIST OF FIGURES